HANDHELD STAND-ALONE MICROFLUIDICS COMPATIBLE FIELD-USE FLUOROMETER FOR MEASURING THE CONCENTRATION OF ANALYTES IN A SAMPLE

By

Matthew Anctil

RECOMMENDED:

Dr. Brian Rasley
Committee Member - Biochemistry

Dr. Andrej Podlutsky
Committee Member - Biology

Dr. Kelly Drew
Committee Member - Neuroscience

Dr. Cheng-fu Chen
Committee Chair – Mechanical Engineering

Dr. Rorik Peterson
Department Chair – Mechanical Engineering

APPROVED:

Dr. Douglas Goering
Dean, College of Engineering and Mines

Dr. John Eichelberger
Dean of the Graduate School

12/17/15
Date

# HANDHELD STAND-ALONE MICROFLUIDICS COMPATIBLE FIELD USE FLUORIMETER FOR ANALYZING THE CONCENTRATION OF ANALYTES IN A SAMPLE

A

THESIS

Presented to the Faculty

of the University of Alaska Fairbanks

in Partial Fulfillment of the Requirements

for the Degree of

MASTER OF SCIENCE

By

Matthew Anctil, B.S.

Fairbanks, AK

December 2015

## Abstract

This thesis presents the work performed to produce a handheld fluorometric tool for the analysis of microfluidics lab chips. The first section of this thesis describes the methods used for the design and development of this fluorometric tool. Each of the major components was tested individually to determine how effectively it would perform under different circumstances and configurations. Compensations were made for the weaknesses identified in each of the major components. The second section describes the laboratory testing of the developed photofluorimeter. Initial testing was carried out using a photo fluorescent tracer dye known as fluorescein sodium salt. Additional testing was performed using D-glutamic acid as a target chemical and 2,3-naphthalenedicarboxaldehyde (NDA) as the marker fluorophore. The resulting fluorimeter was capable of reading fluorescein and NDA labeled D-glutamic acid at the single μM concentration level. The data show a linear relationship between sample concentrations and the readings provided by the sensor.

# Table of Contents

Page

# List of Figures

Page

# List of Tables

Page

# Acknowledgements

I would like to thank Dr. Cheng-fu Chen for his continued support as the committee chair and committee members Dr. Brian Rasley, Dr. Andrej Podlutsky, and Dr. Kelly Drew for their guidance and assistance. Finally, I would like to thank my wife Mallory Jaie Anctil for all her love and support. Part of the thesis work was supported by the Mechanical Engineering Teaching Assistantship, Biomedical Learning and Student Training (BLAST) scholarship, and the National Aeronautics and Space Administration (NASA) under Grant Number NNH15ZHA003C.

# Chapter 1. Introduction

## 1.1.Background

### 1.1.1. Microfluidics

Microfluidics is the field of manipulating fluids using channels in the micrometer size range. The study of such fluid manipulation has potential to aid in the development of the chemical, and biological sciences [1]. On microfluidics, Kuznetsov [2] states:

> Microfluidics deals with the behavior, precise control and manipulation of fluids that are geometrically constrained to small, typically sub-millimeter, scales. It is a multidisciplinary field intersecting engineering, physics, chemistry, microtechnology and biotechnology, with practical applications to the design of systems in which such small volumes of fluids will be used. The behavior of fluids at the microscale can differ from 'macrofluidic' behavior in that factors such as surface tension, energy dissipation, and fluidic resistance start to dominate and properties such as inertia and convection become negligible.

Microdialysis is a sampling technique used to continuously monitor compounds in living tissue. It has a wide range of applications in the biological sciences, biological engineering, and neuroscience. Microdialysis is inherently related to microfluidics and is an emerging application field of microfluidics technologies. Microdialysis uses theories from microfluidics to conduct dialysis at the sub-millimeter scale. In the conventional usage current microdialysis devices have a relatively large sampling volume, which often leads to a prolonged sampling time. Therefore, miniaturization of microdialysis sampling devices is in demand, in order to achieve better temporal and spatial resolution. Professor Chen (University of Alaska Fairbanks) recently used theoretical calculations and predictive modeling to show that a miniaturized microdialysis chip could improve the spatial and temporal resolution of microdialysis "by one order of magnitude or better" [3].

Microfluidics devices such as microdialysis probes are often manufactured by soft lithography. Soft lithography refers to a family of techniques for fabricating or replicating structures using "elastomeric stamps, molds, and conformable photomasks" [3]. The "soft" refers to the use of elastomeric materials, such as PDMS (Polydimethylsiloxane), in manufacture. When cured, PDMS is a soft, transparent polymer. Soft lithography is generally used to construct microscale features in part due to the low cost of the polymer and the quick curing time which makes soft lithography a fairly inexpensive fabrication technique.

### 1.1.2. Spectroscopy

Spectroscopy is an analysis method utilizing the characteristics of chemicals which absorb light radiation at various wavelengths. Spectroscopy can be divided into several categories based on the excitation method and the detection method. Spectroscopy has seen various and abundant use in research fields such as forensic sciences, biology, chemistry and biochemistry as expensive bench-top machines. Spectroscopy comes in many forms including emission, and absorption spectroscopy.

This research is focused on fluorescence spectroscopy because of its simplicity and relatively low cost. Photo fluorescence is a phenomenon in which a chemical absorbs light energy by raising an electron to a higher energy and releases light energy at a different frequency when the electron collapses back to a stable position, as shown in Figure 1.1.

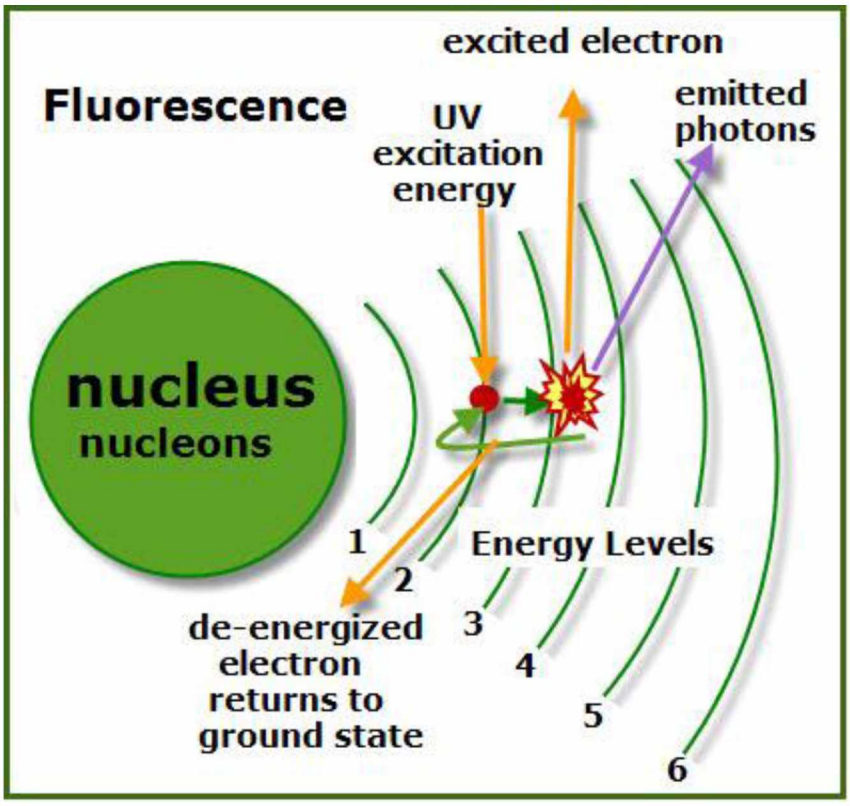


Figure 1.1: Illustration of how fluorescence works on a molecular level [4].

In the fluorescence process, higher energy light is absorbed and lower energy light is emitted effectively converting light energy of one wavelength or color into another. Using fluorescence spectroscopy, one may use the intensity of the emitted light to determine the concentration of a fluorescent chemical or marker in a sample.

Fluorescence begins when a molecule absorbs energy from a photon with a compatible wavelength causing the energy from the photon to transfer to an electron raising the electron's energy level. In this elevated energy state, the electron is unstable and eventually falls back to a stable orbit. In the process of falling, electromagnetic energy is released in the form of light radiation. The emitted light energy typically has a different wavelength and lower energy than does the excitation light.

### 1.1.3. Applications

Discrete sampling of analytes using photoluminescence techniques has a wide range of applications in biological, chemical, and clinical sciences. This research is focused on the biological sampling of chemicals produced by cells. Abnormal production activity from a cell or group of cells is detrimental to the health of an organism and can be the result of infection or genetic or epigenetic mutations. Many biological chemicals have been discovered and markers have been developed to identify several of these chemicals, either to a unique chemical specifically or to a family of chemicals. These markers are often used in Enzyme Linked Immunoassays (ELISA). Using this technique not only allows the user to determine quantitatively the concentration of a particular chemical or chemical family in a sample, but also to see a real time response to a given stimulus by identifying concentration changes. Discrete real-time sampling of a living culture of cells is a novel technology which will be of great benefit to many areas of study in biological sciences.

The handheld photofluorescence detection device (photofluorimeter) developed in this thesis work can be used in combination with one or several microfluidics chips. The purpose and design of the microfluidics chips may vary based on the target chemical, but any chemical that can be individually and specifically labeled with a fluorophore can be quantitatively measured with this photofluorimeter. Limiting the size of the photofluorimeter and the required sample means it could be used in a manner such as a diabetic blood sugar test: passing a single drop of whole blood through a microchannel chip or a series of chips to separate the blood constituents and analyzing the component of interest such as the plasma or white blood cells. A portable photofluorimeter capable of performing discrete real time sampling of the products of living cells would provide medical practitioners with limited resources an affordable tool with which they could monitor a patient's disease progression or reaction to medical treatments such as anaphylaxis. They could also provide various results to the patient in less than an hour without having to send a fairly large sample to a lab for processing. In essence, such a photofluorimeter would bring a portion of the lab into the examination room or into emergency field service.

## 1.2. Literature Review

Color and fluorescence detection has played a major role in biomedical and environmental standards research in recent years [2, 5-8]. Spectrophotometers (color sensors) and fluorimeters (fluorescent light measuring sensors) are often used to interpret colored chemical samples in research labs, diagnostics labs, and ecological and environmental studies (e.g., for chlorophyll in plant leaves). The focus for these color sensors has recently turned to miniaturizing these devices. Recent advances in the field of point of care (POC) microfluidics based diagnostics equipment include devices such as multiplexing enzyme assays for screening newborns for lysosomal storage diseases and diagnostics apparati for identifying markers for a variety of congenital and contracted diseases [1, 6-12]. These advancements are reducing diagnostic times and increasing the sensitivity of existing diagnostic techniques; however, diagnostic tools for emergency response or continuous use in regions without power are extremely limited.

An individual receiving appropriate secondary care before arriving at tertiary facilities (i.e., a hospital) has an increased chance of recovery over one who does not [13]. Including these microfluidics devices in the tool kit of emergency medical services workers could improve recovery rates for patients suffering from unknown ailments. Similarly, attending physicians in rural or remote medical facilities using these tools would be capable of running diagnostics at a low cost and beginning appropriate treatment on a same-day basis.

Currently, the medical field lacks efficient point of care (POC) technologies which are small enough to be carried as a standard tool, efficient enough to operate under their own internalized power systems for dozens of hours of use, quick enough to use in emergency situations, and powerful enough to perform a variety of diagnostic tests. The basis of this research is to develop such a tool, which should be capable of assisting medical professionals in both the military and civilian sectors with POC observation and preliminary diagnosis. This handheld photofluorimeter will combine several different technologies to achieve this goal, including laser induced fluoroscopy microfluidic technologies and low power microcontrollers. To accomplish this goal, a device must be made which is portable, easy to use, and capable of detecting a variety of ailments.

The three major considerations of portability for any field use tool are weight, size, and longevity. Microfluidics devices are small and light by nature, so the remaining consideration is longevity. Longevity includes both the physical durability of the device as well as the battery life for tools with electronic components. Therefore, the goal in this category is to remove these diagnostics tools' dependence on external power supplies.

In order to accommodate the ability to detect a variety of ailments, a novel approach has been taken to unify various microfluidics technologies by designing a modular microfluidics system. A modular system allows the user to connect a single chip or a series of chips to the sensory device based on the function(s) of the chips and the needs of the patient. Using a modular design expands the functionality of the sensory device as new chips are developed without the need to redesign or purchase a new sensory tool.

Fluorimeters are commonly used in field surveys of plant life to measure chlorophyll content in plant leaves. These devices have been reduced in size and can be considered portable enough for field use; however they remain fairly large and cumbersome and require a significant power supply as seen in Figure 1.2.

Figure 1.2: Portable chlorophyll fluorimeter PAM-2500 [14].

Some newer designs have been patented, and even fewer have been implemented to produce a smaller, more energy efficient fluorimeter for field use; however, none have been found to be a completely stand-alone device. Several of the newer field use designs incorporate a smartphone as an integral component [11, 12]. Using a smartphone in the fluorimeter design has the added benefits of using a high powered portable computer as the display, software, power

source, and sometimes the optical sensor all in one prefabricated package; however, it also has several drawbacks. While smartphones are readily available in most parts of the world and millions of people own them, they are not the ideal platform for field service fluorimeters.

Smartphones come in many brands and each brand has its own connectors, ports, and power needs. The different physical configurations include the volumetric measurements of height, width, and length, as well as curvature, screen size, port positioning, and port type. Because of these physical differences, a universal phone cradle would be difficult to design and may not be compatible with future designs. Just as smartphones come in several physical configurations, they also come with different operating software systems including Apple, Android, and Windows. For a device to work with a phone, appropriate software must be provided so that it will be able to use the processor. To provide service across all platforms, multiple softwares must be provided and maintained to keep up with the constant operating system updates for each platform. The need for indefinite programming maintenance unnecessarily increases the cost of the device and decreases its reliability. The batteries installed in smartphones have a limited lifetime and cannot be replaced in some models. This means that a new phone would eventually be needed to run the fluorimeter, and as stated before, the newer models may not be compatible. Other designs include computer software so that the fluorimeter can be run on a laptop. This option is also impractical because a secondary, battery-operated device is required to run the apparatus, making it a mobile bench-top model, which limits its portability.

LOC (Lab on a Chip) technologies have become very popular in the past few years. Many of these fluorescence-detecting devices utilize microfluidics in conjunction with other technologies to perform a task that would otherwise require the use of several technologies, typically bench-top laboratory tools. LOC chips are self-contained and typically perform a specific series of tasks to conduct an assay. Some of these LOC technologies require an analysis device to interpret the assay results. While the smartphone apparati have taken a step toward providing a common analysis tool for multiple test chips, they are still custom-designed for an small, exclusive set of tasks.

While searching through several patents and existing products, it was observed that several different excitation methods were employed for various luminescence detection devices

including X-ray, chemo-, electro- and photo-excitation. Three of these devices appear to be usable as portable fluorometric devices, [15-17]. The electrochemoluminescent detection device developed by Azimi et al. [16] is a sophisticated microfluidics device primarily designed as a DNA/RNA analysis device. It is a well-designed piece of laboratory machinery but lacks the simplicity and speed required for emergency or real time diagnostics. The universal sample preparation system developed by Jovanovich et al. [15] states that it fits into an enclosure of no more than 10 $ft^3$, which is still quite large. This device also requires a computer. These features also restrict the use of this system in remote locations or emergency situations. The measuring device developed by Suzuki [17] makes no mention of a computer or processor which uses input from the sensor to provide data, or of a specific power or light source. This ambiguity leaves the measuring device a component of a system and not a fully developed stand-alone analysis apparatus. As far as physical designs of these devices are concerned, nothing novel has appeared within the last decade. These patented mobile devices share similar designs with existing optics technology, such as lenses, concave mirrors, and mirror orientation. The miniaturization of the optics technologies and the incorporation of unique microfluidics chips and analysis software make the devices more portable. Photo excitation appears to be the most popular method among the portable devices because it is the least invasive, as well as the most simple to implement.

Photo excitation-based fluorescence analysis apparati appear in various forms, but the standard functions are the same. The excitation light acts upon the sample, which absorbs the exciting photons and re-emits the energy as photons with a different wavelength, which are then read by a photon-capturing sensor. In most designs, the excitation source line of sight and the sensor line of sight are orthogonal in order to reduce photons from the excitation source contaminating the sensor. In some cases, this design does not work due to the geometries involved, and a linear orientation is used. In these devices, either reflective or absorbing light filters are used to restrict the wavelength(s) of light allowed to pass onto the sample and the sensor [18]. Additional lenses, prisms, and mirrors are often included to collimate or focus the light throughout these devices. This is the case for the portable fluorimeters mentioned before. However, a more effective tool is available for light collimation. This tool is known as an integrating cavity. Integrating cavities are used in high precision bench-top analysis machines, which are capable of measuring the quantum yield of fluorescence. Utilizing this technology will

simplify the design of a portable fluorimeter as well as allow the device to detect very small concentrations [5, 12, 18-21].

A fluorimeter with these capabilities would not be restricted to POC and emergency medical applications. When paired with an appropriate microfluidics chip, this fluorimeter could be used to detect the concentration of any substance labeled with a fluorescent chemical. With the development of appropriate microfluidics chips, this device could also be used in a variety of applications in a broad array of fields, including emergency medical response, standard medical care, law enforcement, biomedical research, veterinary practice, and wildlife studies.

## 1.3. Scope

The goal of this thesis is to produce and test a handheld photoflourometer for a quick assessment of analytical contents labeled by fluorescence-emission substances. This portable detection apparatus should be self-contained with a long service life and a high level of sensitivity at an acceptable resolution. It must produce results in less than one hour and be able to integrate or interconnect with other microfluidics chips. While none of the methods or procedures used in this research are new, the combination of these technologies and techniques makes this work novel. Microdialysis is widely used to sample molecular substances from the extracellular fluid of organisms. When combined with other analytical tools such as capillary electrophoresis (CE) and laser induced fluorescence detection (LIFD), microdialysis can accurately identify and distinguish multiple types of molecules. However, it can be expensive and time-consuming. Combining these technologies into a single system and miniaturizing the microdialysis component means that readings may be attained very quickly, perhaps in real time. Rapid, consecutive readings allow for analysis of reactions to stimuli for closer examination. This ability to obtain results quickly and build up a database of discrete real time samples could prove beneficial by allowing medical professionals to provide results on a same day schedule or to observe a patient's reaction to new medications, disease progression, or diet and chemical imbalance issues.

The scope of this project is to develop a miniaturized photofluorimeter capable of determining the concentration of target analytes with low power consumption. A modular microfluidics design is proposed to facilitate the use of a variety of assays via microfluidics chips for the fluorimeter. Potential analytes may be any chemicals which are suspended in a fluid, including cytokines and amino acids in extracellular fluid or a prepared solution.

# Chapter 2. Apparatus Design

## 2.1. Design Considerations

From the literature review, it is apparent that there are a variety of fluorometric devices with different limits of detection, a variety of excitation methods, and a few commonly used source/sample orientations for sample excitation and reading. The source of excitation energy may differ from one model to the next based on the specific objectives of said tool. In general, many of these devices arrange the excitation source and detector in an orthogonal orientation with the sample positioned at the intersection. Other models use an in-line orientation with the excitation energy source, sample, and detector arranged coaxially [18].

Several design criteria must be considered to meet the goals of this thesis work. Acquiring a sensor of an appropriate size can help reduce contaminating light from the excitation source and ensure that the light emissions from a low concentration of fluorophores will be enough to trigger the sensor. Because this experiment is specifically focused on the detection of samples in microchannels, the optical sensor should be similar in size to the sample to allow the entire surface area of the sensor to capture the photons emitted from the sample.

When considering the battery life of a portable device, the processor often consumes the majority of the power. The microcontroller provides the computing power necessary to operate the photofluorimeter as well as controlling power consumption, which will enable a longer battery life for the photofluorimeter. The fluorophore-based sensing also provides the photofluorimeter with a medium for presence and concentration detection without the need for image processing software or complicated machinery, which reduces the power demands of the system.

The excitation source is another power-hungry component, so it must be chosen carefully to limit power consumption. This decision also ties in with the simplicity of the photofluorimeter. There are several different sources of molecular excitation energy. Here we

discuss two of the simplest methods of introducing electron excitation energy to fluorescent molecules.

1) Electrical excitation is the most direct and efficient method of chemical excitation. However, power electronics are required to control the amount of current passing through the sample. Because the fluorimeter is intended for use with a variety of fluids and fluorophores, additional control circuitry would be required to adjust the excitation current to each sample and chemical, because the electrical properties may differ between samples.
2) Photon or light excitation is the simplest method of chemical excitation. The fluorophore takes in as much energy as it can from the photons hitting it and excess photon energy is simply reflected or passes through the solution. With photon excitation, no additional circuitry is required, and the power level need not be altered for every sample.

A photon-based excitation energy source was chosen for its simplicity. In many conventional photofluorimeters, a monochromatic laser is used as the light source. This is undesirable for this portable design because standard lasers are fairly large and require a large power source. LEDs are capable of producing high levels of light with a relatively low cost of power when compared with other light emitting devices. By using an LED as the light source, the goals of low power consumption, long physical life, and small size can be met. However, LED light sources emit broad spectrum light. The light is not restricted to a single wavelength like traditional monochromatic lasers. Therefore, when using an LED light source (in this case an LED laser) for the purpose of fluorometric analysis, light filters are required to restrict the band of wavelengths absorbed by the light sensor to those emitted by the sample and not the source.

## 2.2. Materials

### 2.2.1. Color Sensor

In order to detect fluorescent emissions, a color sensor, photometer, or spectrometer is required. These light sensors come in various packages and designs. Among a few technologies for differentiating different wavelengths of light and measuring light intensity, photodiodes were chosen in this thesis work for their low cost, high level of repeatability, and linear response to light intensity.

Table 2.1: Comparison of several different light sensor types and their performance in a variety of categories [22].

| Electrical Characteristics | Photo-multiplier Tubes | Photo-diodes | Photo-transistors | CdS Photocells | Other Photo-conductors | Integrated Circuits | Hybrids | Sensor Electronic Assembly |
|---|---|---|---|---|---|---|---|---|
| Available Wavelengths (μm) | 0.2-0.9 | 0.2-2.0 | 0.4-1.1 | 0.4-0.7 | 2-15 | 0.2-15 | 0.2-15 | 0.2-15 |
| Performance-to-cost Ratio | Fair | Good | Excellent | Excellent | Fair | Fair | Fair | Good |
| Sensitivity | Excellent | Very Good | Very Good | Very Good | Very Good | Very Good | Very Good | Very Good |
| Linearity | Good | Excellent | Good | Good | Good | Good | Good | Good |
| Ambient Noise Performance | Fair | Very Good | Very Good | Very Good | Very Good | Excellent | Excellent | Excellent |
| Dynamic Range | Very Good | Excellent | Very Good | Good | Good | Very Good | Very Good | Very Good |
| Stability | Very Good | Very Good | Good | Poor | Fair | Very Good | Very Good | Very Good |
| Other Characteristics | | | | | | | | |
| Reproducibility | Fair | Excellent | Fair | Poor | Fair | Very Good | Very Good | Very Good |
| Cost | High | Low | Very Low | Very Low | High | Medium | High | Medium |
| Ruggedness | Poor | Excellent | Excellent | Excellent | Good | Excellent | Very Good | Excellent |
| Physical Size | Large | Small | Small | Small | Small | Small | Medium | Medium |
| Ease of Customization | Poor | Easy | Fair | Fair | Poor | Poor | Poor | Fair |
| Lead time for Customization (weeks) | 40 | 12 | 14 | 12 | 20 | 40 | 30 | 16 |

Excluded from Table 2.1 are two types of light sensors commonly used in digital cameras: CMOS (complimentary metal-oxide semiconductor) and CCD (charged coupled device). Modern CMOS sensors are commonly used for their comparable performance to CCD and their lower power consumption. Funding permitting, a CMOS sensor would be preferred for the construction of this handheld photofluorescence detection device.

The selected photodiode sensor for this thesis work is the Avago ADJD-S311-CR999 color sensor (Avago Technologies, San Jose) (Figure 2.1). The sensor's package dimensions are 2.2 × 2.2 × 0.76 mm. It has a BGA (ball grid array) connection lead scheme using 0.25 mm diameter hemispherical attachments in a 3 × 3 square grid with 0.56 mm on center spacing (Figure 2.1(a)). Its photodiode array is 0.42 x 0.42 mm (Figure 2.1(b) multicolored area). Although its diminutive size makes it difficult to work with by hand, this particular sensor was chosen because it uses photodiodes, and its size is suited for microfluidics applications (Figure 2.1(c) sensor size relative to a quarter).

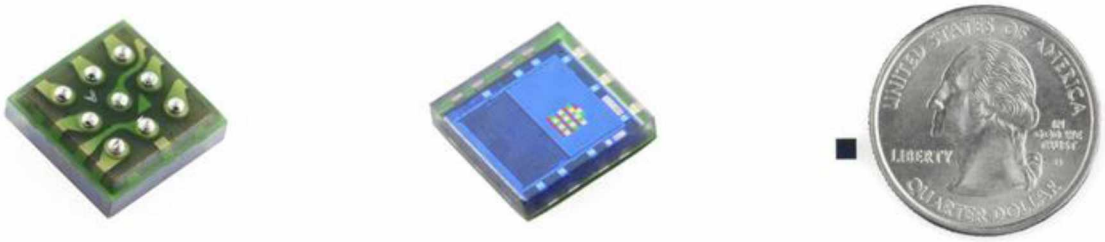


(a) (b) (c)

Figure 2.1: The Avago ADJD S311-CR999 color sensor. (a) ball grid array, (b) color sensor, (c) Comparison of the Avago ADJD S311-CR999 color sensor with a quarter.

The working principle of the color sensor is to use photodiodes to absorb photons and allow the electrical current to flow through the diode. An array of photodiodes is arranged on the surface of the sensor. These photodiodes are equipped with red, blue, and green light filters (see Figure 2.2).

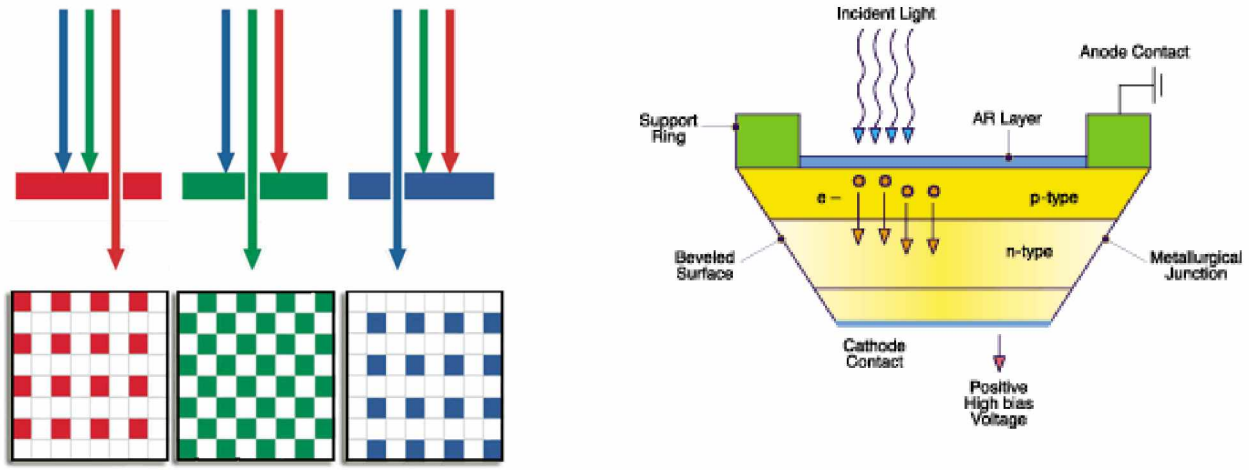


(a) (b)

Figure 2.2: Illustration of how the photodiode color sensor works [23, 24].

For this particular sensor, the blue and green light filters share a band of frequencies because the cutoff regions of the band pass filters are tapered instead of abrupt. This means that without further filtering, some light from the blue source could contaminate the results. The software used with the sensor requires a calibration against a white standard and gives four output values, one for each set of photodiodes. These four values represent the level of intensity of the red, blue, green, and visible light bands in a 10-bit resolution, in which 0 represents an undetectable level, and 1023 represents saturated electronics as a maximum readable value. Because this project deals mainly with fluorescein, the green value is of the most interest. For consistency in calibration, a stand with a piece of white cotton was made to provide a matte white surface at a consistent distance from the sensor. The sensor board also includes an onboard white LED source, which was used for the calibration.

The substrate of the sensor board is a printed circuit board (PCB) on which electrical connections replace wires in a compact and stable platform for bonding electrical components to make a functional module. Most commercial PCB companies use photolithography to produce copper wire traces on FR4, which is a composite material with Fire Rating of 4 consisting of

glass fiber reinforced epoxy laminate sheets. This technology was used to make a mold for the PDMS polymer microchannel chip.

### 2.2.2. Excitation Source

The excitation source was chosen to be an LED laser. This decision was made because LEDs are well known for their low cost, longevity, and low power consumption. LED lasers differ from standard laboratory quality lasers, which are monochromatic and coherent, due to their use of artificially grown precious and semi-precious crystals or gasses such as ruby and argon as a gain medium. LED lasers use an LED as a light source and a series of lenses as a collimating mechanism. LED light is not monochromatic, meaning that it emits a broad spectrum of light wavelengths (Figure 2.3). Because the LED lasers are not monochromatic, light filters are required to isolate narrow bandwidths of desired light emissions.

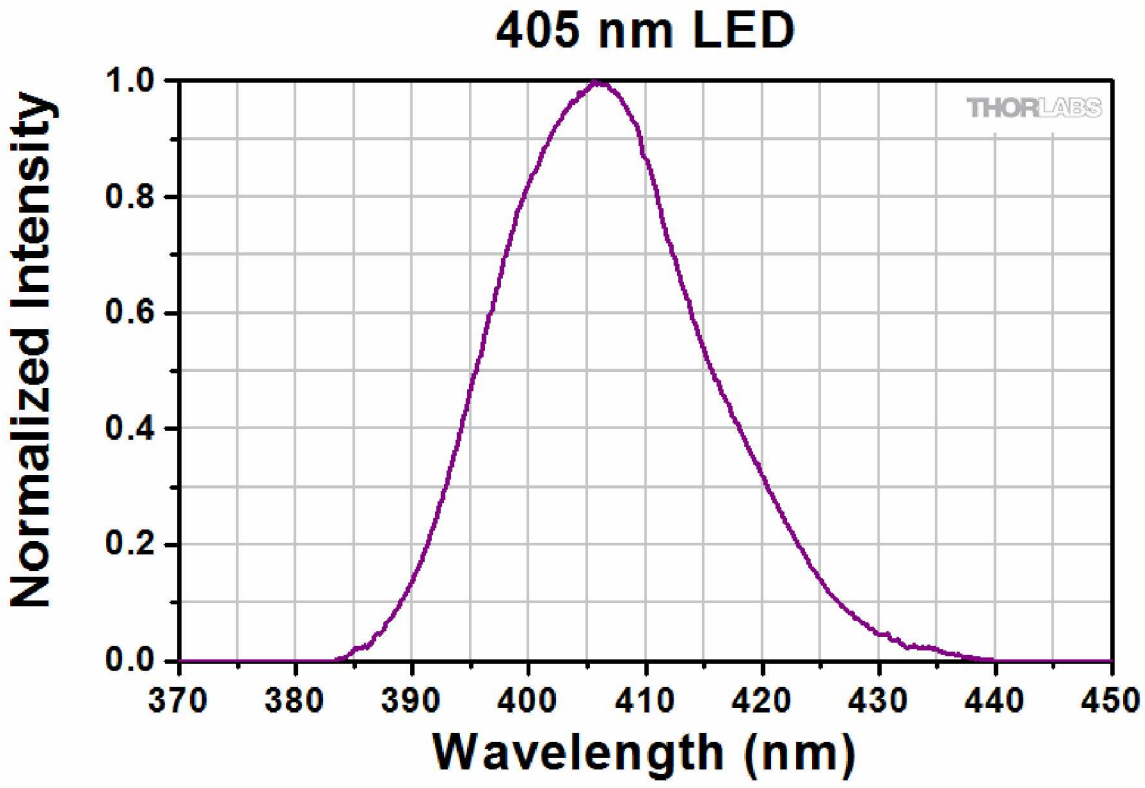


Figure 2.3: Typical output spectrum of a 405 nm LED.

The ideal configuration for this photofluorimeter using an LED light source would be to place a filter over the light source before it interacts with the sample, and another filter after the sample emits the light. Due to a limited budget, only one light filter was purchased. This filter was placed between the sample and the color sensor. In an effort to minimize light pollution, the aforementioned green band pass filter was purchased and an LED light source was found which did not emit light in the 500 – 540 nm bandwidth.

The light filter used in this work (Figure 2.4) was purchased from Thor Labs online [25]. It is a band pass light filter, meaning that it blocks or reflects all light except for a small selected band. The light filter used for this work has a central pass wavelength of 520 nm and a pass band width of 40 nm. This means that light of wavelengths between 500 and 540 nm passes through the filter, while light with wavelengths falling outside this range is blocked. A 405 nm LED laser provides enough energy to excite the fluorescein sample without emitting light in the 500-540 nm range.


Figure 2.4: Light filter purchased from ThorLabs [25].

### 2.2.3. Microcontroller

A microcontroller is a low power computer with its own memory, input and output peripherals, and processor core, all combined into a small integrated chip package [26]. These small computers allow a user to regulate the power consumption of a device by controlling how and when the computer communicates with the peripheral devices, such as light sensors, and when these peripherals turn on and off. This ability to reduce power consumption to a minimum makes a microcontroller the ideal computer for a field use device.

Several makes and models of microcontrollers are available for purchase. Typically, the differences in models from the same manufacturer are in the peripherals included on the board on which the microcontroller is mounted. These peripherals determine to what each board is better suited. An Arduino UNO microcontroller board was chosen for this work because it is a commonly used general purpose hobbyist microcontroller and because operating software for the ADJD S311 color sensor was available as freeware for the Arduino Uno board [27].

### 2.2.4. Reflective Cavity

To improve the resolution of the fluorescent emissions detection, an integrating reflective cavity was used in the photofluorimeter. Mirrors were used to craft a light container in an attempt to capture the light emitted by the fluorescent molecules and increase the sensitivity of the photofluorimeter. A mirror finished spherical interior cavity would be preferable; however, with the tools available, flat plastic mirrors were more practical for custom construction. The mirrors used were 1/8" thick polycarbonate plastic with one side covered in standard silver mirror coating. The edges were beveled to 45° in an attempt to make a continuous mirrored surface. The interior of the cavity is a $3\times3\times3$ $in^3$ cube.

### 2.2.5. Test Analytes

For testing, this portable photofluorimeter is used to measure two fluorescent materials in vitro. The first is fluorescein sodium salt (Sigma-Aldrich, St. Louis, Mo) [28], which is chosen as a model fluorophore because of its high emission intensity, common use in biological studies, affordability, and small molecular size. Fluorescein salt has a molecular weight of 376.27 g/mol with a solubility of 500g/L in water. The peak excitation wavelength of fluorescein is 490 nm and the peak emission wavelength is 515 nm. An optimal pH value for fluorescent activity is 9; however, buffers were not readily available for regular testing, so deionized water with a pH of 4.5-5was used.

The second material measured is D-glutamic acid, a naturally occurring amino acid which was used in the final experiment as the biological sample of known concentration to be labeled with a fluorescent marker and analyzed with the apparatus. 2,3-naphthalenedicarboxaldehyde (NDA) was used as a fluorescent marker to label the D-glutamic acid for analysis.

## 2.3. Design of Experiments

The fluorimeter was designed by testing the components separately to observe any non-ideal behavior before integrating the pieces together. There were four major stages of development for this photofluorimeter. The first stage of development was to test the fluorescein, the light source, and the sensor. The second stage was to test different orientations and spacing of the apparatus for the best detection result. The third stage was to improve the resolution of detection and reduce the deviation in detection. The fourth stage was to test biological samples in vitro using a different fluorophore. Each stage is described individually in the following chapters

# Chapter 3. Stage-1 Development

## 3.1. The Sensor

The goals for the first stage of development were to: (1) examine the feasibility of using the Avago ADJD S311 color sensor as a fluorescence sensor and (2) develop a sample platform suitable for observation of analytes.

The first task was to attach the sensor to a circuit board for interconnecting with other necessary electronic components. A circuit board was designed in Eagle CAD (free PCB layout software, see Figure 3.1) and was cut using a computerized numerical control mill (see Figure 3.2).

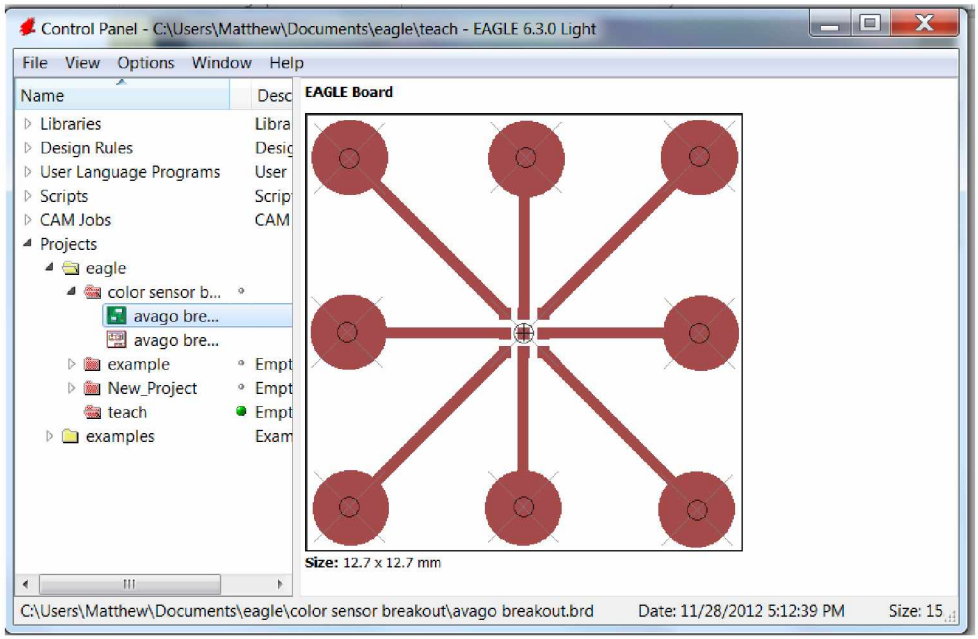


Figure 3.1: Eagle CAD rendition of the PCB for the color sensor.

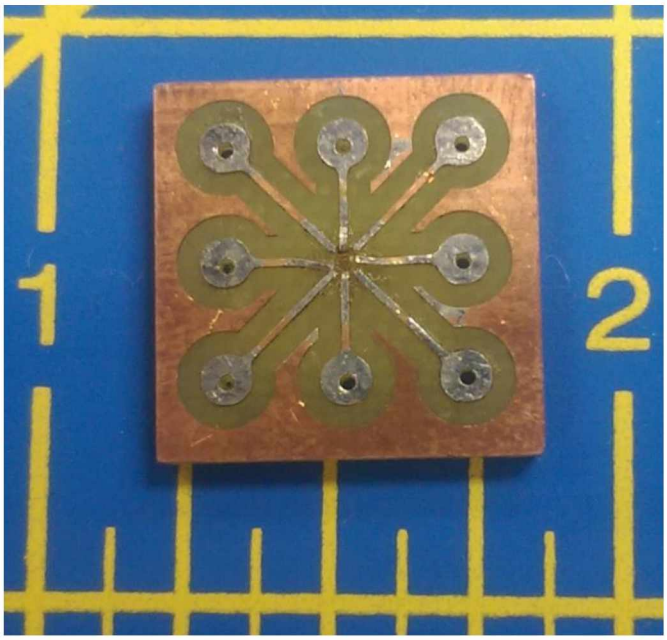


Figure 3.2: Close-up top view of the circuit board before the sensor was mounted.

The sensor is attached to the PCB by soldering its leads in a 3×3 BGA. Soldering this sensor to the PCB is a very difficult task due to the size of the leads. In order to achieve a good solder joint on such a small scale, a sophisticated mechanism known as a hot gas reflow soldering machine was used (see Figure 3.3) to bond the two pieces together (see Figure 3.4).

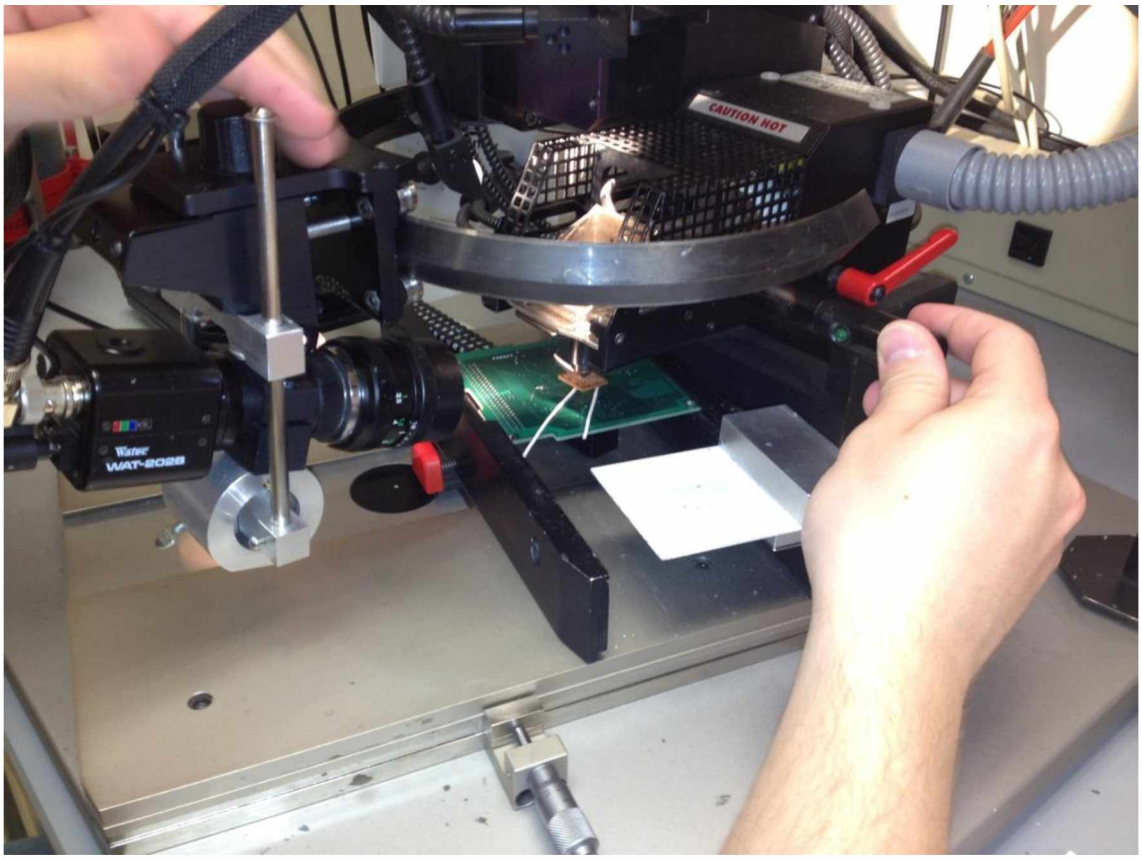


Figure 3.3: Reflow soldering machine. The first attempt at attaching the ADJD-S311 to a circuit board.

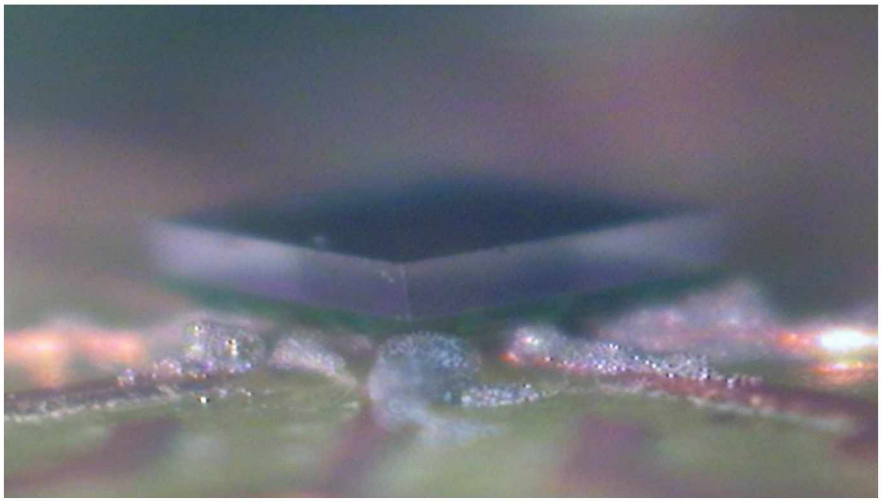

Figure 3.4: Close-up side view of the sensor attached to the circuit board.

The drawback to making a milled circuit board as opposed to a photolithography-made PCB is the relatively wide copper traces and spaces between them. Because of this resolution restriction on the board, the central lead on the sensor was unable to be connected in a conventional manner. Several attempts had been made to attach this lead through a hole in the middle of the circuit board, however, all attempts failed. Having failed at making a customized circuit board for the sensor, a prefabricated board for the sensor was purchased from Sparkfun electronics [27] (see Figure 3.5). This board came with the sensor and all of the required supporting electrical components.

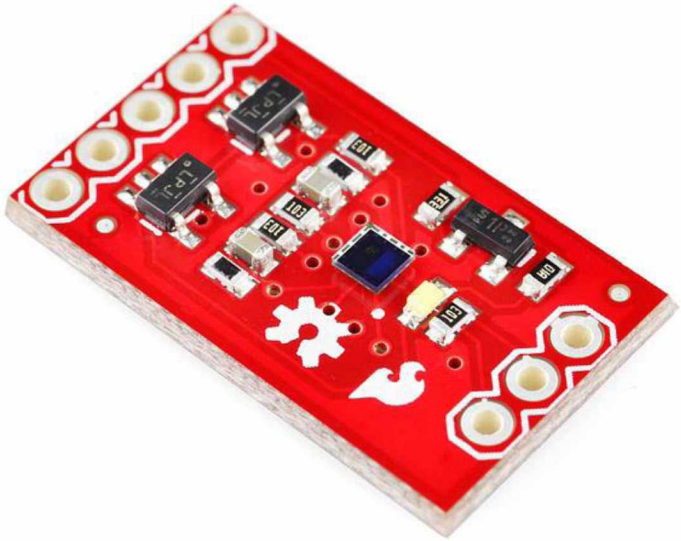

Figure 3.5: Color light sensor evaluation board used in this project [27].

With a working color sensor, the next step was to design and construct a microfluidic chip for containing the fluorescent solution sample. The objective was to produce a microchannel capable of performing microdialysis (for the future application to detect samples obtained by microdialysis), with a viewing window for fluorescence detection. The microfluidic chip is composed of two pieces of molded PDMS. One piece contains a microwell which is replicated using a master mold, shown in Figure 3.6.

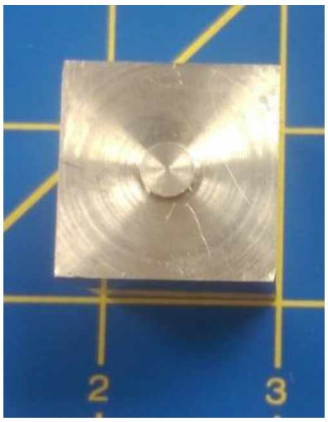


Figure 3.6: Master mold used to make PDMS microwell chips.

## 3.2. Testing the Microdialysis Chip and the Light Sensor

The microwell was filled with a fluorescent solution of fluorescein sodium salt [28] and deionized water in arbitrary concentration for in vitro perfusion. The other PDMS piece contains a microchannel fabricated using another master mold made with PCB copper traces, shown in Figure 3.7 (a). The microchannels were flushed with DI water to perfuse the fluorescent solution from the microwell. To facilitate perfusion of the fluorescent solution (i.e., microdialysis), a serpentine microchannel was designed to fit on top of the microscale well. The serpentine configuration of the microchannel was intended to increase the perfusion time of the fluid passing over the membrane and well. The microchannel design is shown in Figure 3.7 (b).

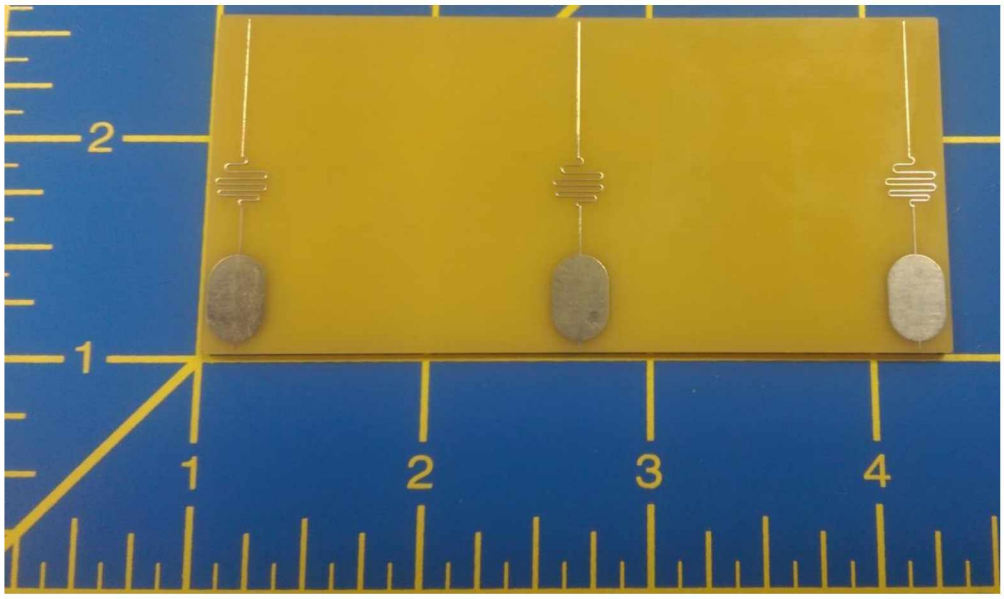


(a)

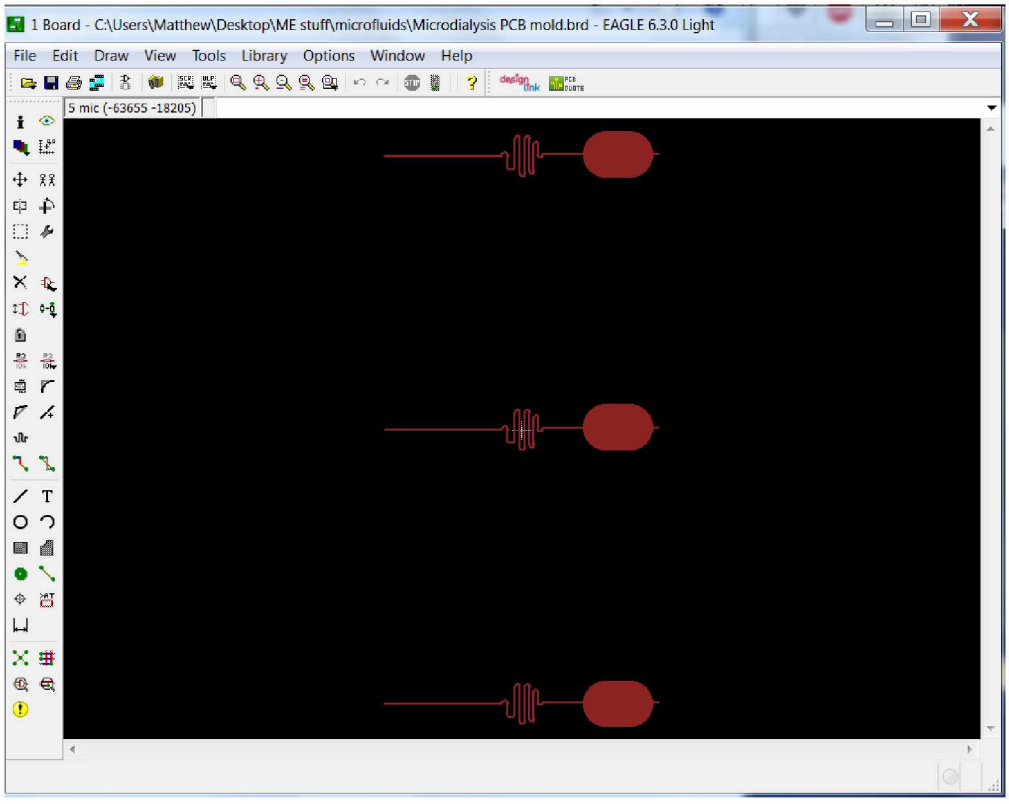


(b)

Figure 3.7: (a) Master mold PCB used to make microchannels in PDMS chip. (b) PCB mold design for fabricating microchannels for microdialysis chip. (Drawn in Eagle CAD.)

Once replicated with the needed microfluidic patterns (the microwell and microchannels), the two PDMS pieces are brought together to sandwich a semi-permeable membrane. We used a polycarbonate membrane with pore size 1 μm in this thesis work for quantitative microdialysis in vitro. To bond the polycarbonate membrane to the PDMS, the membrane was treated with plasma for one minute and submerged in a 5% APTES (3-aminopropyltrirthoxysilane) 95% water solution at 80°C for 20 minutes. The PDMS pieces and the membrane were then plasma treated and pressed together to bond [29].

As can be seen in Figure 3.8, the microwell was made too large and thin, which caused it to easily collapse during the bonding process.

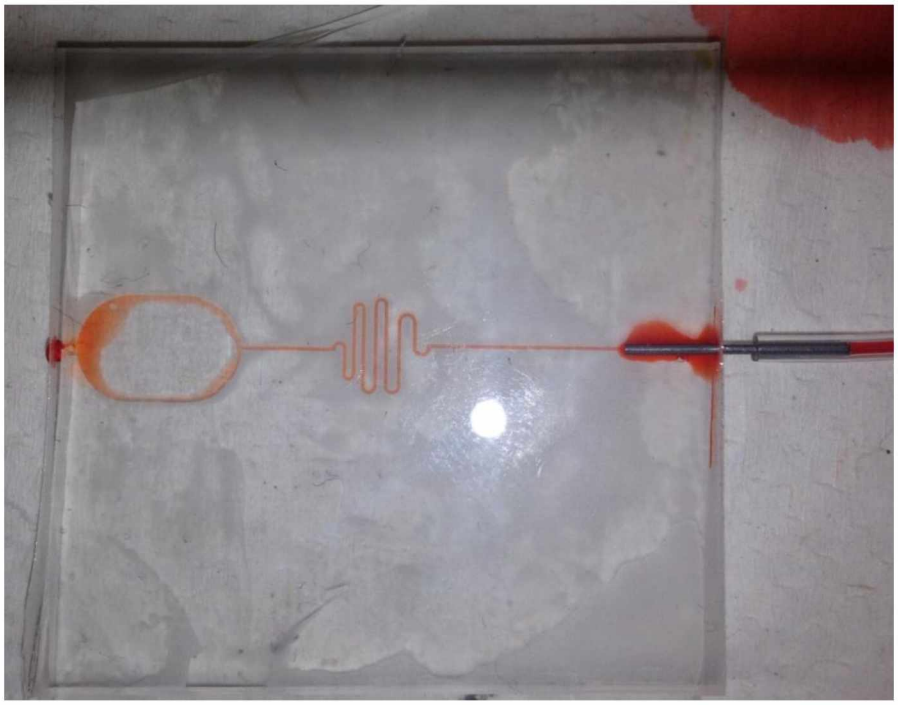

Figure 3.8: Sample microchannel fabricated using PCB mold. The channel and bonding to PDMS substrate were tested by injecting deionized water with red food coloring.

To alleviate this issue, solder was added to the copper plate on the mold to make a dome-shaped cavity which held up better to the bonding process. The resulting chip and viewing window can be seen inFigure 3.9 (b).

(a)

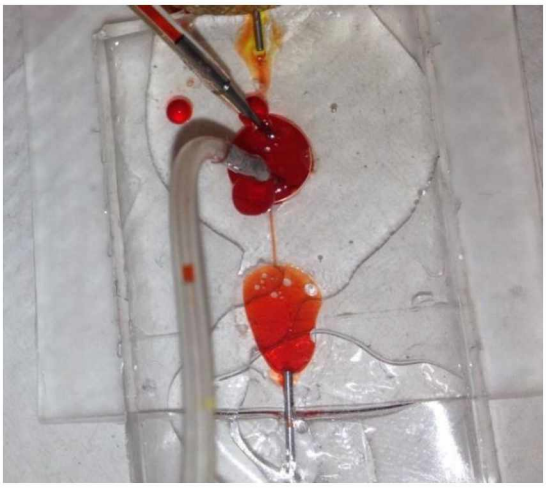

(b)

Figure 3.9: (a) Microdialysis chip fabricated using PCB mold. (b) Microdialysis chip fabricated with additional solder on the PCB mold for the viewing chamber. The channel and its bonding to PDMS substrate with microwell and polycarbonate membrane were tested by injecting deionized water with red food coloring.

Using the configuration shown in Figure 3.9 (b), the microdialysis chip was used in combination with the photodiode sensor for initial testing. In an effort to reduce systematic error, the sensor board and the light source LED were attached to the sample chip. Attaching the electronic components to the PDMS chip required an additional step because PDMS does not bond readily to FR4, copper, PCB laminate, or electrical components. To overcome this issue, the components were completely encased in PDMS. Because of the rough and irregular topography of the electronics mounted to the PCB, the PDMS holds the electronic components solidly and provides a surface for bonding to other PDMS surfaces. The fully integrated microdialysis chip is shown in Figure 3.11.

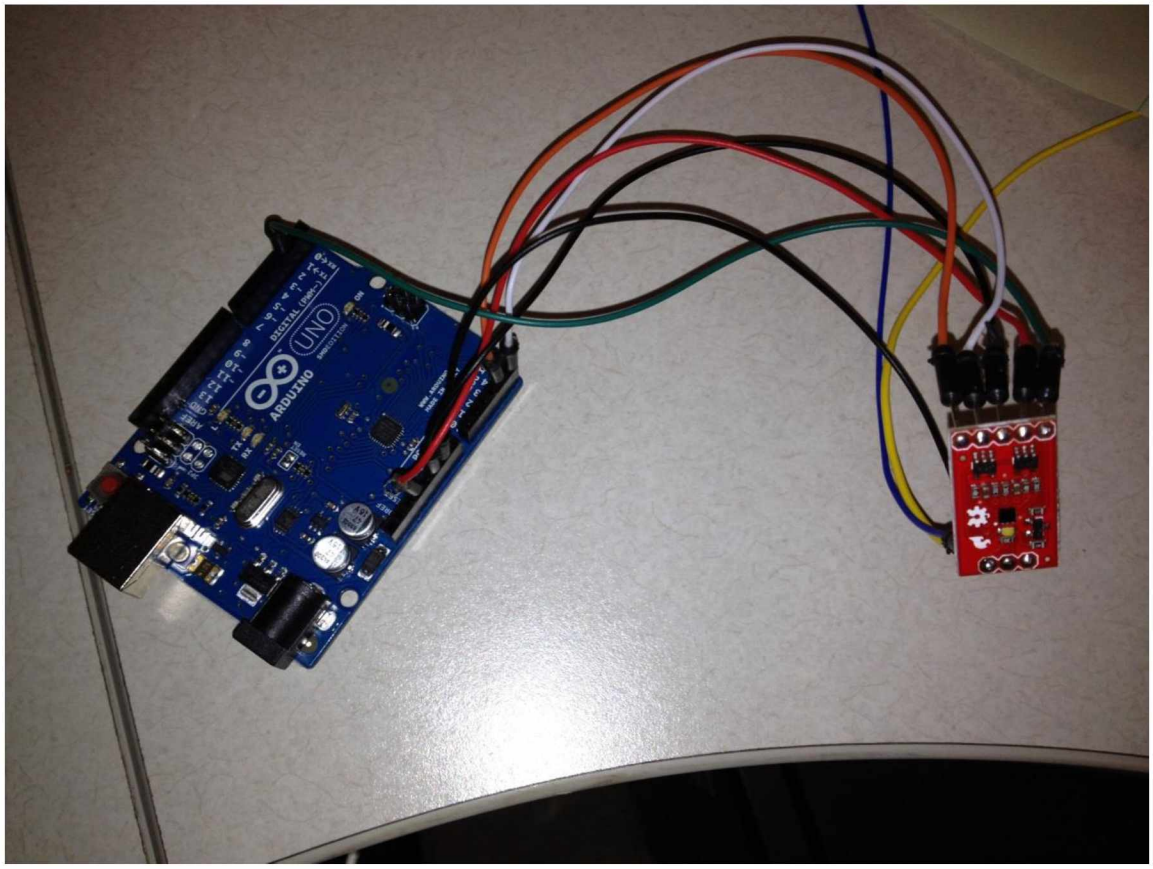


Figure 3.10: Arduino UNO microcontroller board (left, blue) connected to the Avago ADJD-S311 color sensor evaluation board (right, red).

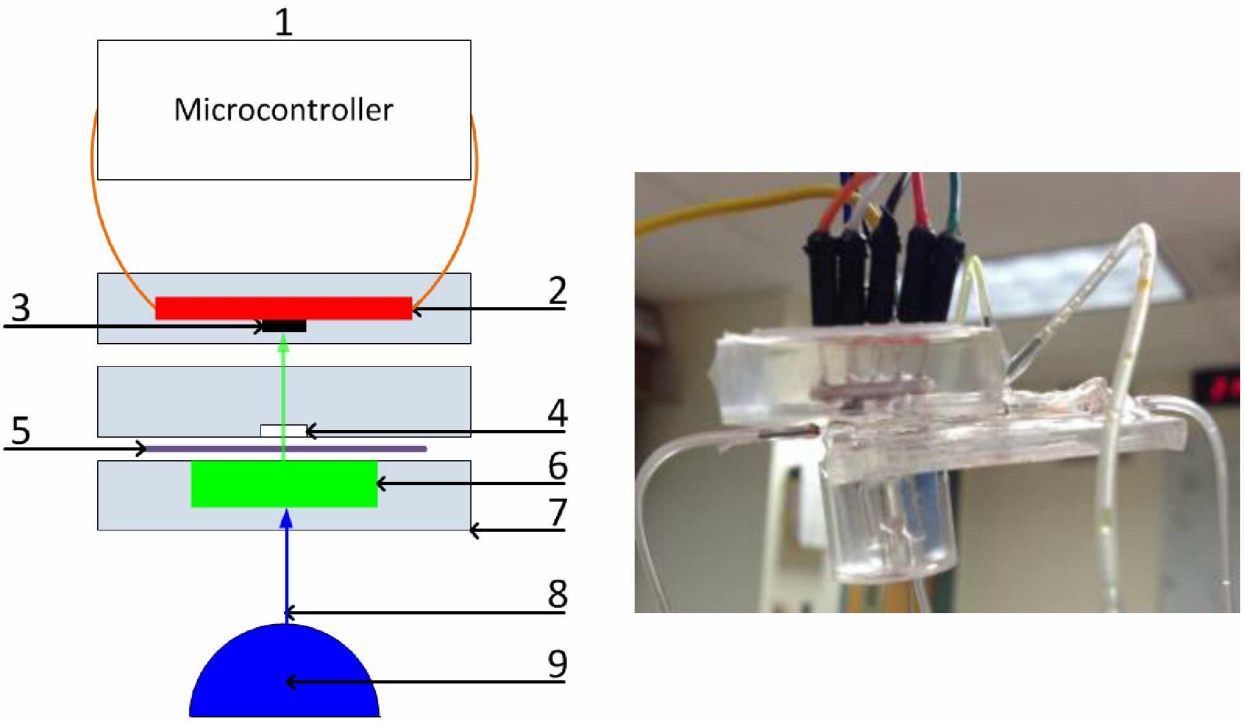


(a) (b)

Figure 3.11: Five layer PDMS microfluids chip consisting of the microcontroller (1a), color sensor breakout board (2a, red), Avago ADJD S311 color sensor (3a, black), microchannel (4a, white), 1 µm pore polycarbonate membrane (5a, purple), microwell (6a, green), PDMS substrate (7a, light blue pieces), light radiation (8a, blue and green arrows), and LED light source (9a, dark blue). (b) Physical model used in experiment.

The initial testing was carried out on a trial run, in which a fluorescein solution at an arbitrary concentration flowed through the microwell and deionized water flowed through the channel. Two outlets were used in an attempt to maintain pressure equilibrium and concentration gradient throughout testing. This can be seen in Figure 3.12, which is a photograph of a trial run using fluorescein and deionized water.

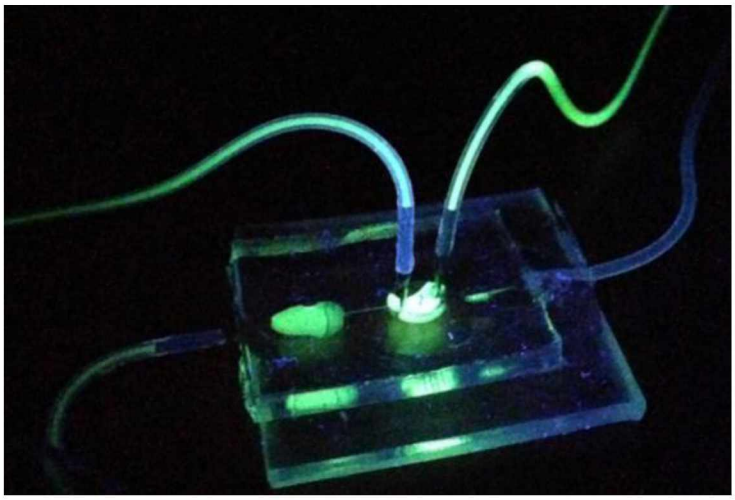

Figure 3.12: Photograph of sample test on incomplete chip. This photograph includes: UV light source (unseen); microwell (bright green circle in the center of the top layer); observation window (green oval, to the left of microwell); two inlets: fluorescein input (top right), deionized water input (middle right); well output (left middle); and channel output (bottom left). A new and complete chip was then constructed and a full test was carried out with the light source and the sensor fixed into place.

The fluorescein input is a very bright green under ultraviolet (UV) light and the deionized water is a very light blue color. The coloration of the water input line may be due to the water having some particulate matter which reflects the UV light or the plastic tubing reflecting the light instead of the water. The output lines and the observation window containing the dialysate solution are a lighter green than the fluorescein input. This visual observation indicates that the microfluidics chip works as desired. The data from these tests is shown in Table 3.1 and the statistical analysis of the data is shown in Table 3.2.

Table 3.1: Readings from flowing two separate samples of different fluorescein concentrations through the chip.

| Calibration number | Inlet | | | | Outlet | | | |
|---|---|---|---|---|---|---|---|---|
| | R | G | B | C | R | G | B | C |
| 1 | 539 | 302 | 796 | 1023 | 293 | 173 | 434 | 734 |
| | 554 | 311 | 810 | 1023 | 298 | 168 | 446 | 792 |
| | 564 | 317 | 830 | 123 | 288 | 166 | 431 | 768 |
| | 564 | 317 | 830 | 1023 | 280 | 165 | 420 | 745 |
| | 569 | 311 | 838 | 1023 | 272 | 162 | 409 | 723 |
| 2 | 167 | 139 | 354 | 603 | 113 | 72 | 237 | 283 |
| | 177 | 136 | 346 | 591 | 121 | 76 | 232 | 285 |
| | 182 | 132 | 337 | 576 | 123 | 78 | 227 | 307 |
| | 191 | 138 | 283 | 484 | 129 | 82 | 193 | 232 |
| | 208 | 140 | 297 | 503 | 140 | 88 | 199 | 351 |

Table 3.2: Statistical analysis of the data in Table 3.1

| Inputs | Red 1 | Green 1 | Blue 1 | Red 2 | Green 2 | Blue 2 |
|---|---|---|---|---|---|---|
| Avg, $C_{in}$ | 558 | 311.6 | 820.8 | 286.2 | 166.8 | 428 |
| Stdev | 11.94 | 6.15 | 17.30 | 10.35 | 4.09 | 14.09 |
| Outputs | Red 1 | Green 1 | Blue 1 | Red 2 | Green 2 | Blue 2 |
| Avg, $C_{out}$ | 185 | 137 | 323.4 | 125.2 | 79.2 | 217.6 |
| Stdev | 15.51 | 3.16 | 31.47 | 10.06 | 6.10 | 20.14 |
| Relative Recovery ($=C_{in}/C_{out}$) | **0.33** | **0.44** | **0.39** | **0.44** | **0.47** | **0.51** |

The data from Table 3.1 and Figure 3.13: Graph of the data observed from flowing two separate samples of different fluorescein concentrations through the chip. show that the green value read from the dialysate solution is about half of the value read from the sample solution. Using the data shown in Table 3.2, the average relative recovery is about 4.3, and the standard deviation increases with higher concentrations, ranging from 3.1 to 31. These results prove the concept of using the simple color detector to quantitatively detect concentration levels of

fluorescent particles; however, they also shed light on several design flaws in the chip and the sensor.

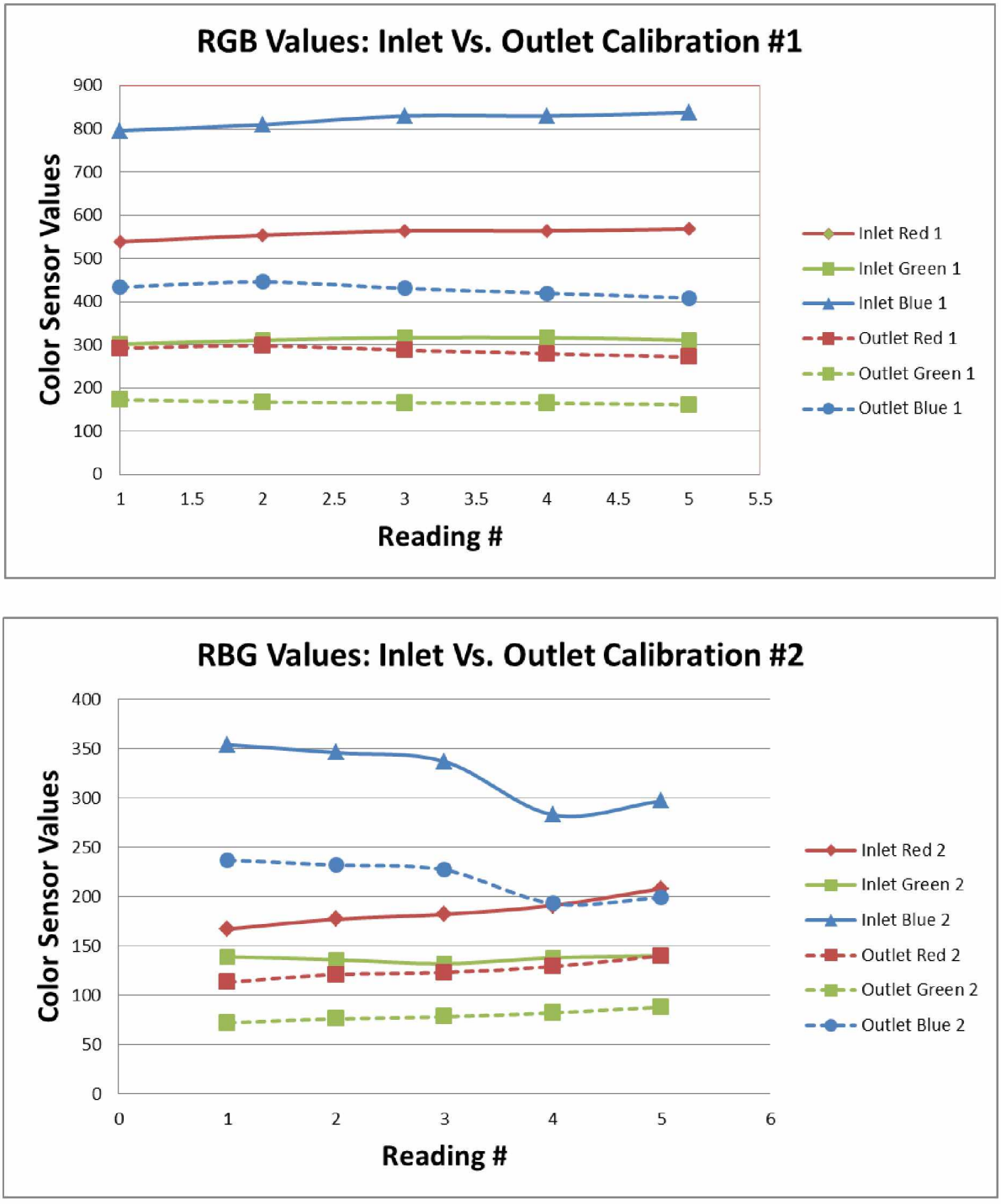


Figure 3.13: Graph of the data observed from flowing two separate samples of different fluorescein concentrations through the chip.

### 3.3. Results, Observations and Redesign of Stage-1 Development

Several issues became apparent from analyzing the results of the fluorescent solution perfusion test. The first issue was that the microdialysis region does not maintain equal pressure on both sides of the membrane due to the different surface areas on either side. This imbalance caused permeation of fluid from the higher pressure side to the lower pressure side. In testing, the pressure on the DI water side was higher, so the water flowed directly through the membrane into the fluorescein microwell. This water permeation changed the concentration of fluorescein in the microwell. Such fluid transportation is undesirable in microdialysis. The second issue was that with the sensor and light source directly bonded to the chip, the chip could not be disposable. To remedy this issue, a new sensor apparatus design was necessary for housing the light source and color sensor in such a manner that samples may be accepted and held in a consistent position relative to the light source and color sensor for repeatable measuring. The third issue observed was that the UV LED provides an undesirable wide spectrum of wavelengths in the blue and even green ranges. On the sensor, the green light filter allows light above 440 nm to pass through, as seen in Figure 3.14.

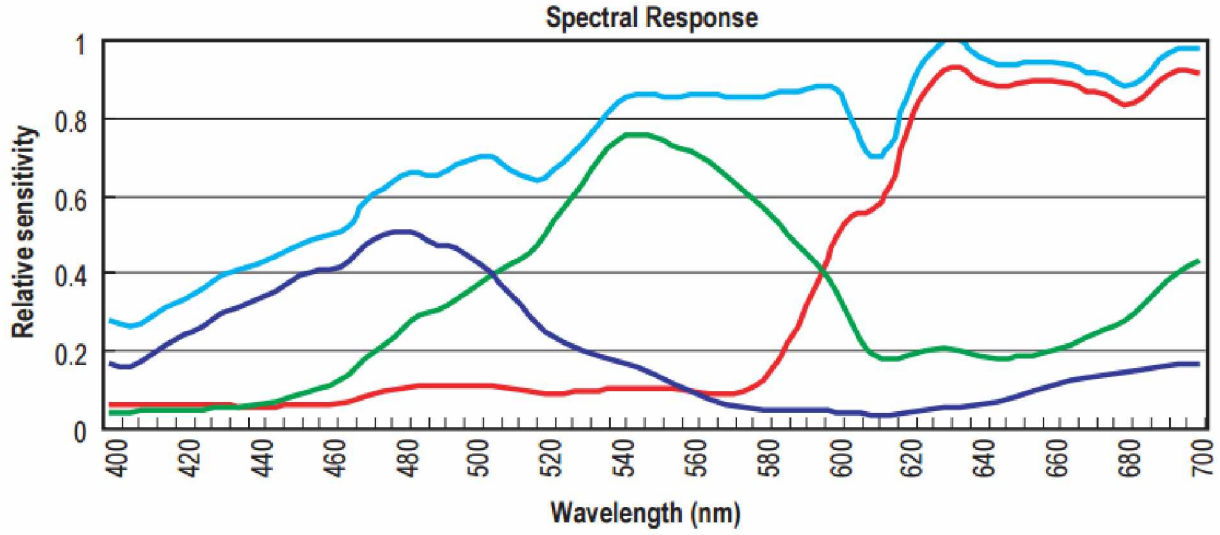


Figure 3.14: Spectral absorptivity of the four filtered regions of photodiodes on the Avago ADJD S-311 color sensor. The light blue represents the clear or unfiltered photodiodes [27].

The dominant frequency emitted by the UV LED was 395 nm. This can cause erroneous readings when the source light comes into contact with the sensor. To remedy this issue, a light filter was introduced into the system, and research was conducted to find frequently used solutions. These considerations lead to the Stage-2 Development.

# Chapter 4. Stage-2 Development

## 4.1. Design and Experiment

Traditional fluorescence detection and some ELISA analysis devices apply the same concepts in the detection mechanism but these concepts are implemented using different approaches. These methods typically place the light source and sensor in one of two configurations: orthogonal or linear. In the orthogonal configuration, the light source and light sensor are placed at 90° to each other, intersecting at the sample. The linear configuration has the source and sensor directly facing each other with the sample in between to form an 180° orientation.

In the design for the second stage of development for this work, the same LED as in Stage-1 Development with a dominant emitted light at wavelength 395 nm was used as the light source. Since the LED light source is not monochromatic, the orthogonal configuration design was chosen in an attempt to reduce contamination of undesired wavelengths from the light source. To collimate the light (as most bench-top devices do), a focusing attachment was made for the LED light source until an appropriate laser could be found. This fixture used a steel tube with a doublet lens mounted to the end opposite the LED to focus the light on a point. The LED lens fixture was mounted to a slot which allowed it to be moved up and down. One advantage of this configuration is that the area of incidence can be altered by adjusting the distance between the source and the sample. Regardless of the configuration of the source and sensor, a band pass light sensor was used to reduce light contamination.

This fixture was tested using a LED with dominant emitted light at wavelength 480 nm, because it is close to the peak excitation wavelength of fluorescein, and with a UV LED with dominant emitted light at wavelength 395 nm. The LED lens fixture and its effects on the light can be seen in Figure 4.1. Figure 4.2 shows the sample chip illuminated from the side by the LED light fixture. When the band pass light filter was applied, it was observed that the 480 nm LED was not a suitable light source, as it emits a high level of light in the 500-540 nm range.

(a)

(b)

Figure 4.1: (a) LED light focusing lens fixture with ambient lights on. (b) LED light focusing lens fixture with ambient lights off.

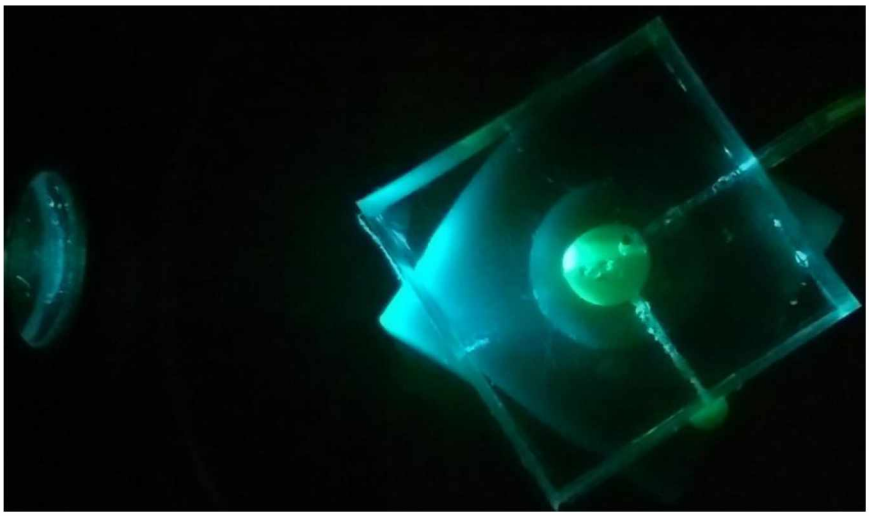

Figure 4.2: LED light fixture test on sample chip isolated from all external light.

### 4.1.1. Testing the Light Fixture

In an effort to evaluate any improvement over the light readings from the testing in Stage-1, a simple microwell chip was used to analyze a sample of fluorescein. The source was held at a constant distance and the light sensor was handheld. Ten samples at decimal serial dilution beginning again from an arbitrarily prepared concentration were used in the microwell chip to perform this test. Figure 4.3 shows the results of this testing.

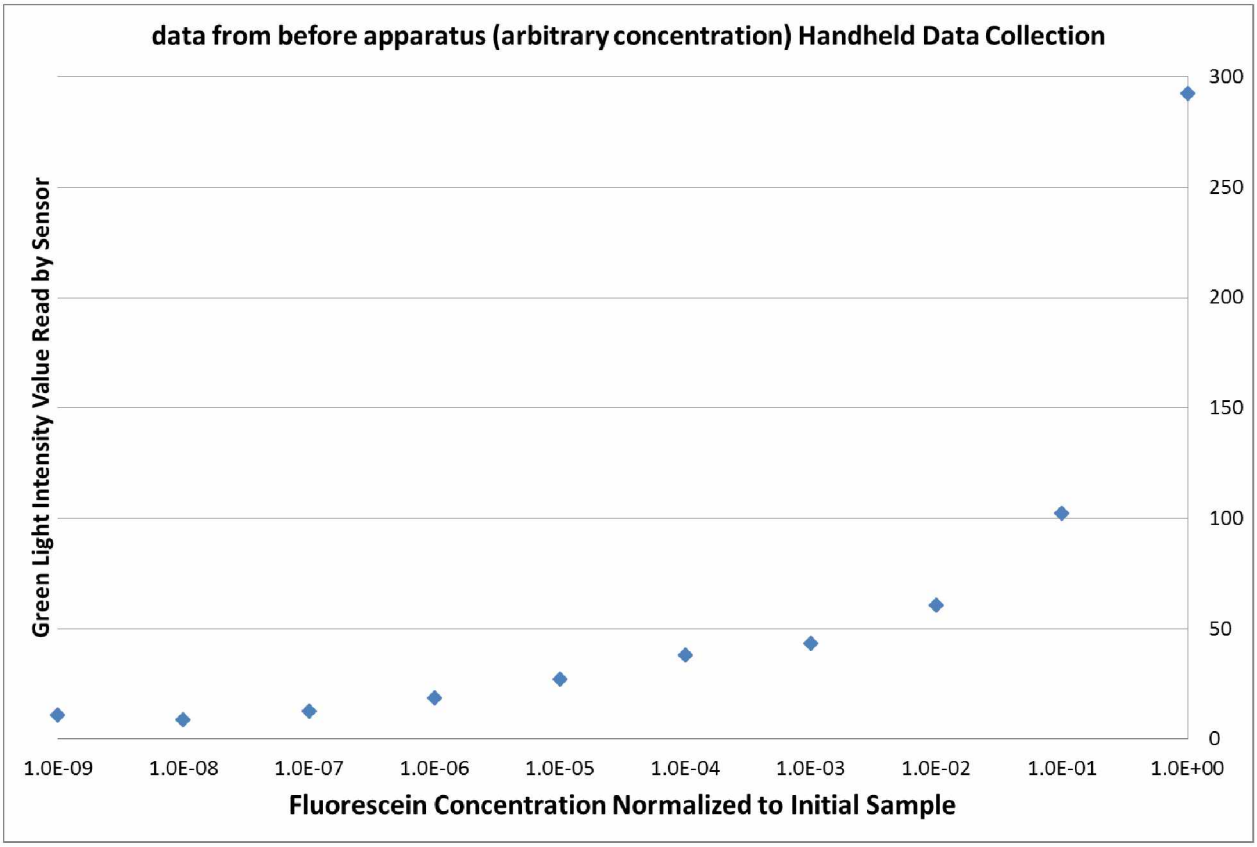


Figure 4.3: Graph of data collected from using the LED light fixture shown in Figure 4.1 and holding the sensor by hand.

This testing showed some improvement over the initial tests and generated a continuous curve. The curve shown in Figure 4.3 demonstrates that the sensor readings are directly correlated to the concentration of fluorescein present in each sample. However, because the sensor was handheld, the results are not reliable as calibration data.

### 4.1.2. Fixture Testing of Orthogonal Lighting/Sensing Orientation

With the data from the handheld tests showing a correlation between sensor readings and sample concentration, an orthogonal fixture was produced from a piece of 90° angle aluminum and a block of HDPE (high density poly-ethylene), as seen in Figure 4.4.

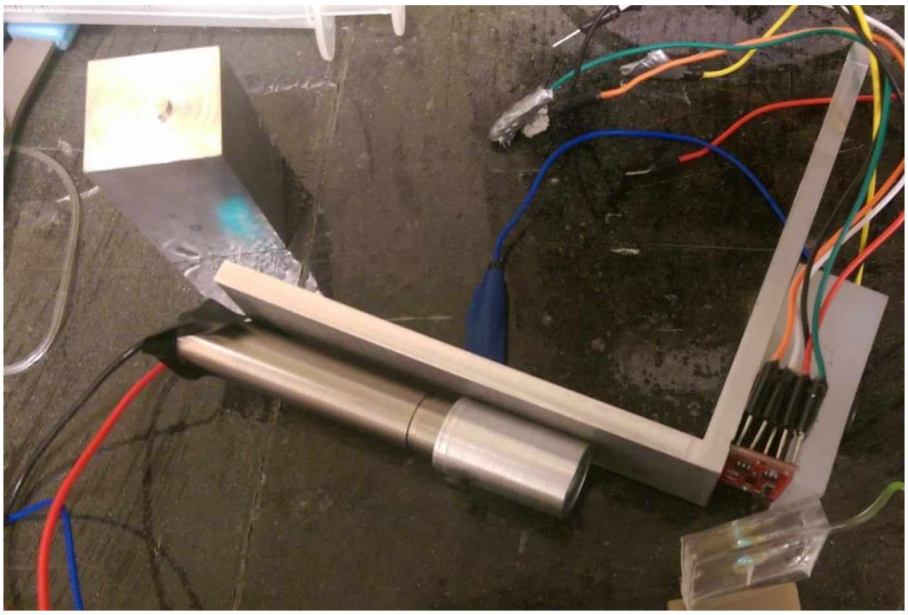

Figure 4.4: Angle fixture with LED light fixture and light sensor attached.

This fixture included a slot to allow the LED light fixture to slide up and down one side. This enables the user to alter the area of incidence between the light source and the sample. This angle fixture did not have any mechanism or platform to hold the sample in a consistent position and so another fixture was made to complete the apparatus, as shown in Figure 4.5. This piece was also constructed from a piece of 90° angle aluminum. With the apparatus completed, another serial decimal dilution set of samples was prepared as shown in Figure 4.6, and run through the apparatus.

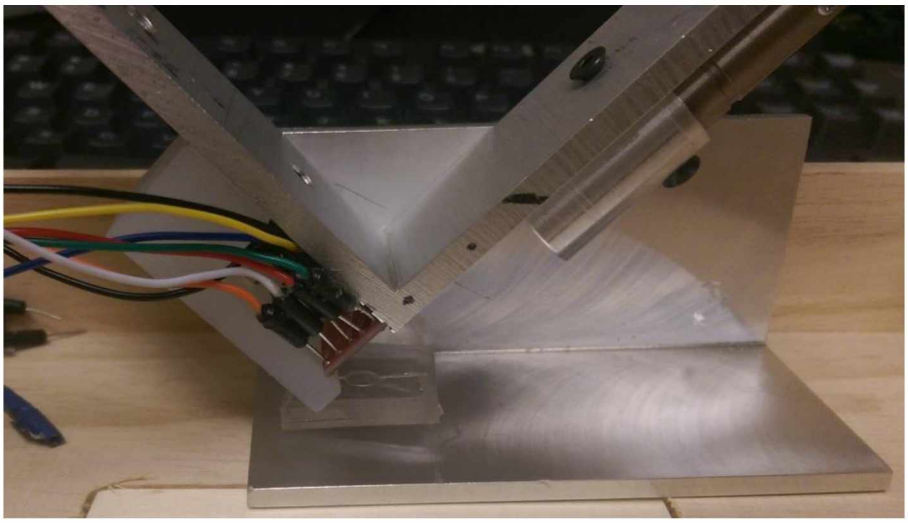

Figure 4.5: Final orthogonal orientation apparatus.

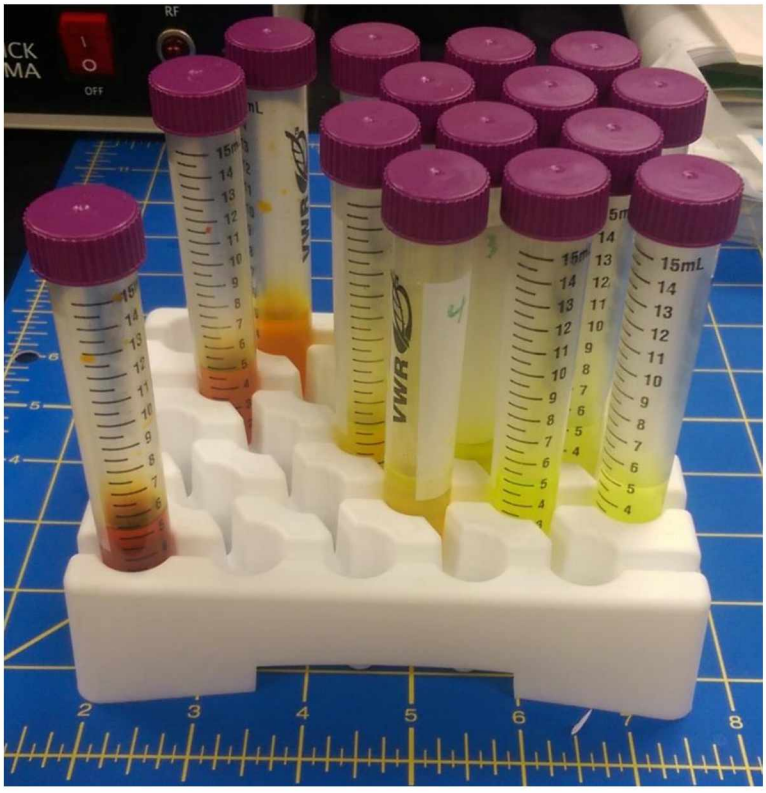


Figure 4.6: Serial 10× diluted fluorescein solutions starting at an arbitrary concentration.

The results of testing were seemingly random and inconclusive as shown in Figure 4.7 (red).

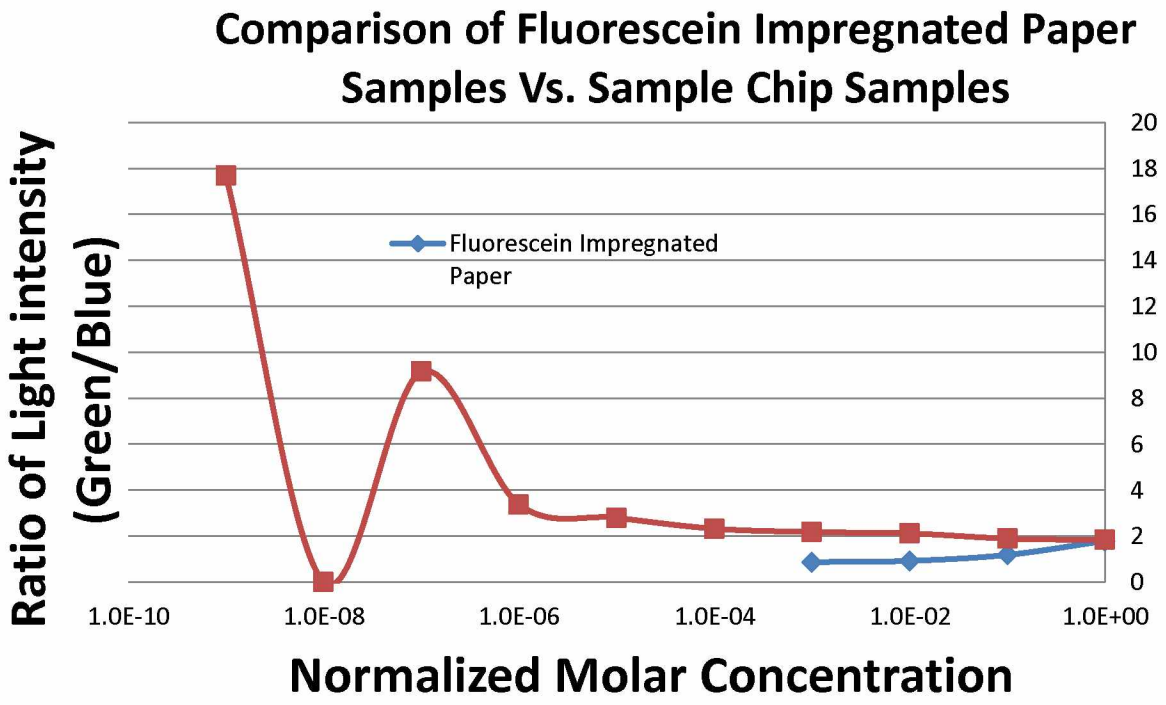


Figure 4.7: Results from tests performed using the orthogonal orientation apparatus.

To determine if the random readings were a result of the interaction between the light source mounted to the orthogonal orientation apparatus (Figure 4.5) and the sample chip, the chip was replaced with a piece of white paper impregnated with fluorescein solution (Figure 4.7 blue).

## 4.2. Observations and Additional Experiment

Another issue observed with this orthogonal orientation apparatus was that the fluorescence emissions propagate in all directions, thus the intensity of light hitting the sensor is considerably lower than the total light emitted. This light scatter can occur in different ways depending on the size of the particle scattering the light. Figure 4.8 shows the radiation effects of light scattering on particles of three different size classes. The types of scattering are separated into two major categories: Mie scattering and Rayleigh scattering [30]. Although the light scatter

phenomenon has discrete classifications, the light scatter pattern changes are gradual and may fall between the styles shown in Figure 4.8. Fluorescein is considered to a small molecule; however, it is considerably larger than the components of air that cause Rayleigh scattering. This means that the light scattering caused by fluorescein falls between Rayleigh and Mie small particle scattering.

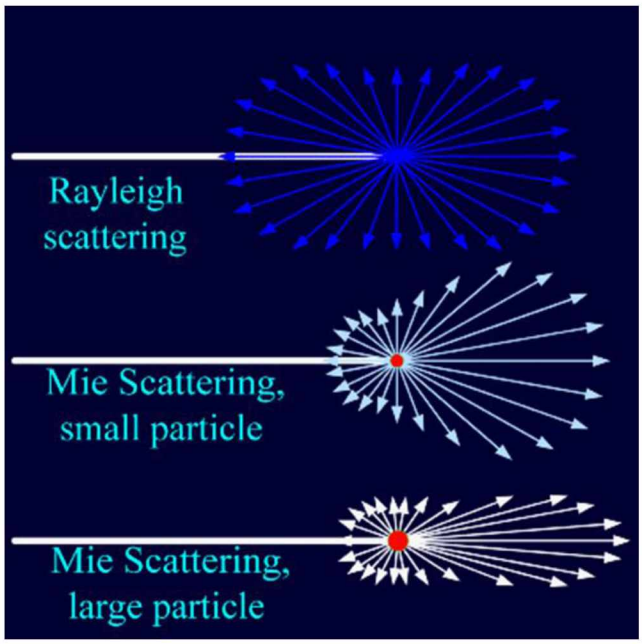


Figure 4.8: Vector representation of different types of light scatter [30].

Because of the light scattering, a light "container" is required to harness as much light as possible from the emitting fluorescent particles. When designing a light container, three basic methods are available: the light can be absorbed, reflected, or bent. Because the quality of the light is important is this case, absorption is not desirable, and bending light at this scale is needlessly complex, so reflection was chosen to contain the light. To test whether a reflective light container would increase the sensitivity of the photofluorimeter, a juice box with a reflective interior was used to approximate a mirrored container (as shown in Figure 4.9), and more tests were run through the chip and compared with the results from the 90° apparatus. The results (shown in Figure 4.10 ) showed higher levels of green light. At this point, no filter had yet been applied, so blue light from the source was also present.

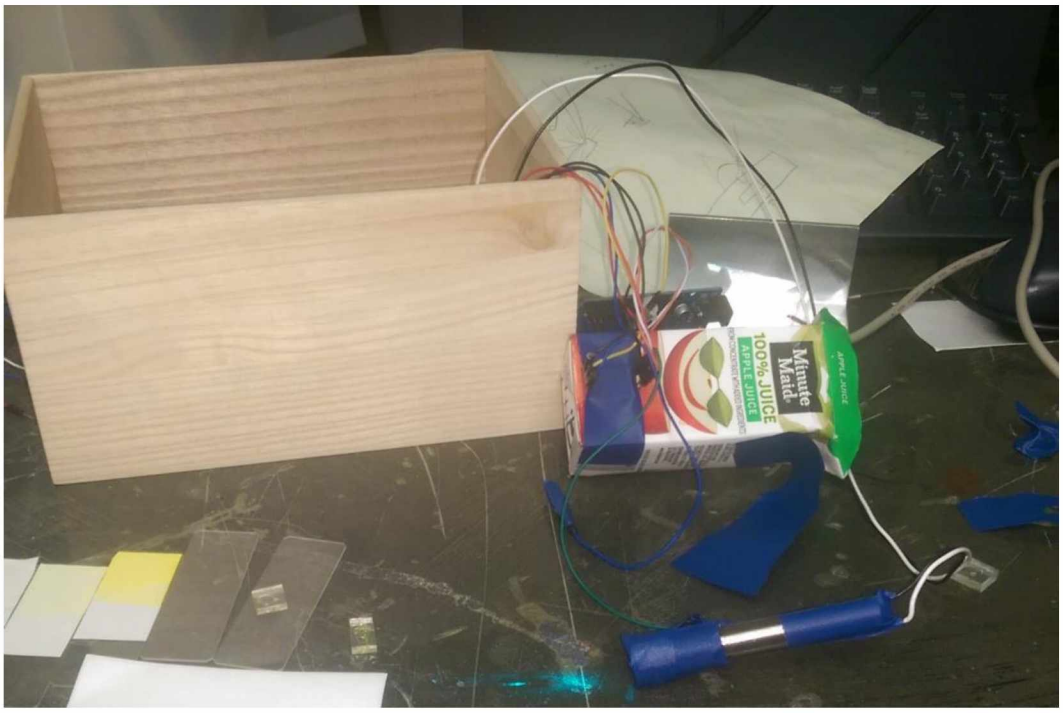


Figure 4.9: Reflective light container made from paper juice box with foil interior.

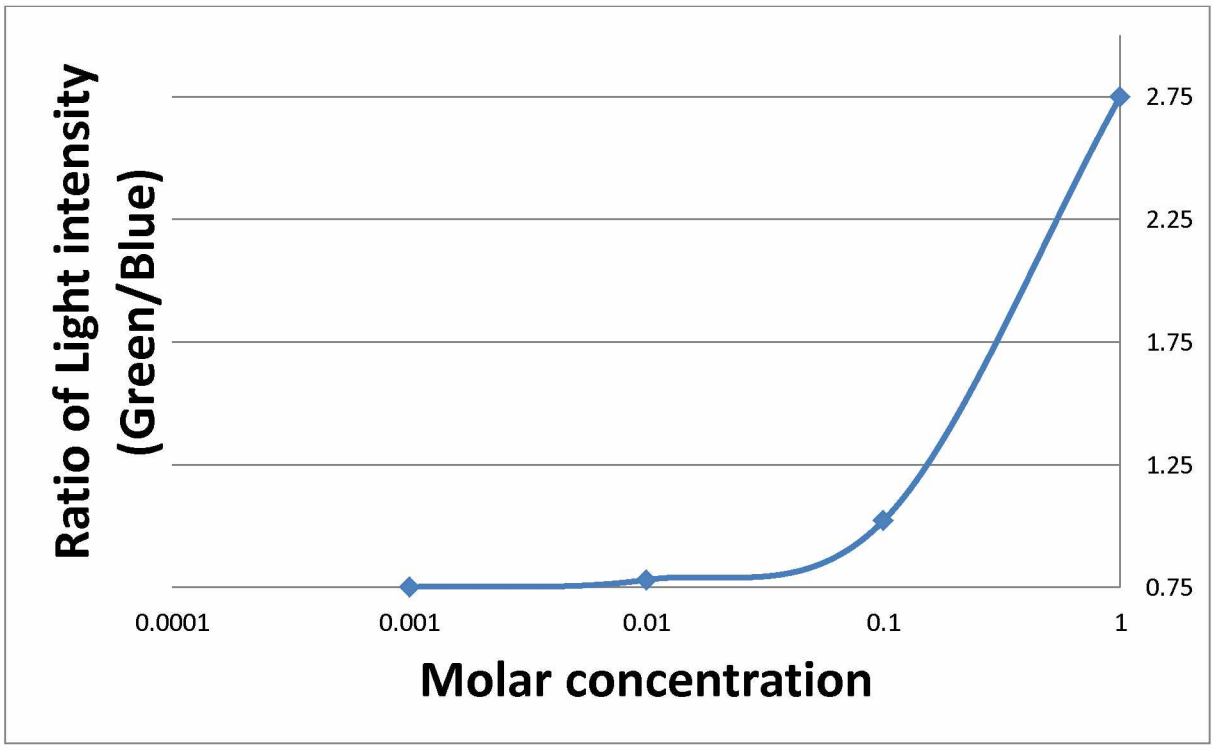


Figure 4.10: Data obtained using a reflective interior juice box to approximate a mirrored container.

## 4.3. Results, and Redesign of Stage-2 Development

The apparatus produced in stage-2 development was incapable of producing consistent results. The primary cause of its inconsistency was that the geometry of the microwell (disc shaped) was not compatible with the orthogonal orientation scheme. Additionally, the way in which the light is scattered reduced the maximum possible sensitivity in the absence of a reflective chamber.

A search for more information on light physics technologies turned up an article on reflective cavities' potential to improve the reliability of results as well as improve the limit of detectable concentrations. It stated that reflective cavities [19], "especially spherical cavities," are a popular design used to "collect and measure the total radiant flux from a source." The article also emphasizes the importance of a reflective cavity in the presence of light scattering for measuring small differences in luminescence. "Its utility is especially important … in the presence of scattering." [19]. This makes the use of a reflective cavity seemingly ideal for the design of this apparatus.

Similar to a standard crystal laser (schematic shown in Figure 4.11), the reflective cavity fixture is comprised of a light source, a reflective box, a small aperture, a gain medium, and an emission wavelength of interest. Some of the major differences between the custom-made fluorimeter device and the standard laser are: (1) the light source is a collimated light passing through an aperture instead of a quartz flash tube around the gain medium; (2) the gain medium is a sample of fluorescent chemicals instead of a crystal; and (3) the exit aperture does not have the 95% reflective mirror which is normally present in a laser. In a laser, this mirror reflects the light inside the reflective chamber until the photons have enough energy to pass through a 95% reflective mirror. In this photofluorimeter, because concentration detection is a major function, this mirror has been removed to allow immediate light intensity values to be observed.

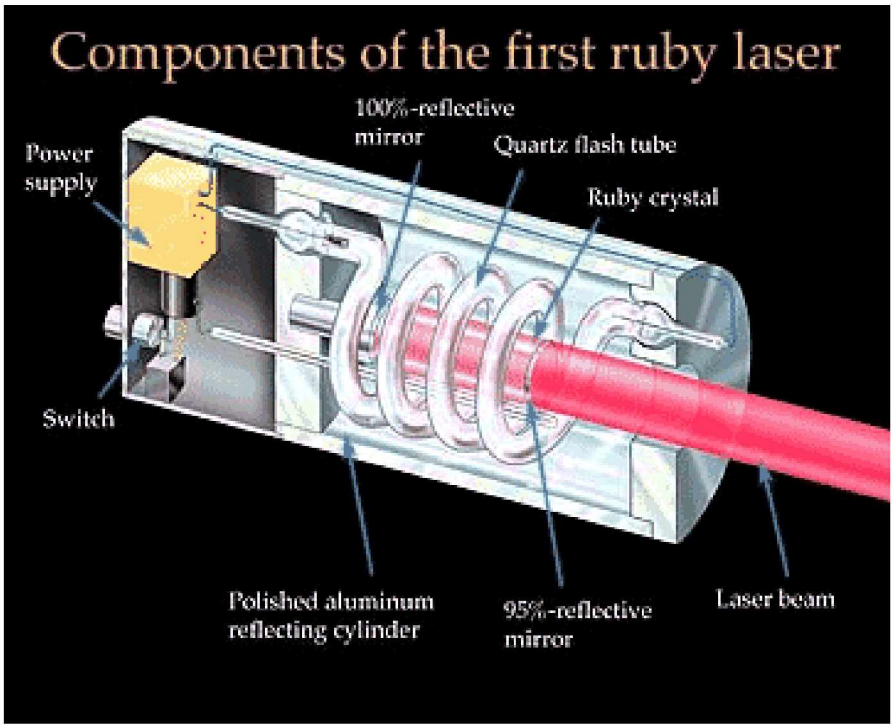


Figure 4.11: Original ruby laser design [31].

# Chapter 5. Stage-3 Development

## 5.1. Design of the Reflective Cavity

For the purposes of this thesis work, a reflective cavity is an enclosed space of a non-specific shape which is reflective on the interior to contain light (e.g., [19]). In the third stage of development, the reflective cavity was integrated into the fluorimeter apparatus to: (1) increase the limits of detection of the fluorimeter; (2) reduce the standard deviation observed between the readings for each individual sample; and (3) produce a photofluorescence spectrometer capable of measuring multiple fluorophores.

In this thesis work, a reflective cavity serves to contain fluorescence emissions and direct the light to a light sensor through a small aperture of the cavity. The shape and size of a reflective cavity are the two major design issues that will affect its quality of assisting in the detection of fluorophores. Ideally, a spherical cavity will serve the best for reflecting the light within it. A cubic shape was chosen to ease the manufacturing rigor, as shown in Figure 5.1, which has a size much larger than it needs to be. The alterations in shape and size make this design less effective in light focusing. The flat reflective surfaces and the rough edges at each side and corner of the mirror plates increase the photon impedance through media and media transition.

The light container was constructed from an aluminum cube base (Figure 5.1, green), to the interior of which standard silver reflective mirrors were adhered (Figure 5.1, purple). A light filter (Figure 5.1, red) was applied to the reflective chamber and a 405 nm LED laser (Figure 5.1, blue) was used to replace the UV LED used in previous stages of testing. This laser is a standard LED laser pen emitting at a wavelength of 405 nm. The cavity was produced by screwing six 3"x3" aluminum plates together. A piece of mirrored polycarbonate with 45° beveled edges was bonded onto each aluminum plate with silicone sealant.

To install the LED laser to the cavity, a hole was drilled at the center of one side of the cavity. Similarly, a smaller hole was drilled on the opposite side of the cavity to serve as the

aperture for mounting the light sensor. The laser was bonded to the cavity using silicone sealant. A sensor chip (Figure 5.1, yellow) was fastened to the outside of the cube with silicone sealant.

A PDMS chip with an open microwell (Figure 5.1, grey) was mounted on the inside of the cavity. The open microwell was for accepting the sample of fluorescence solution. A light filter was placed on top of the PDMS chip. The color sensor chip was then placed directly over the source aperture and the cube was sealed.

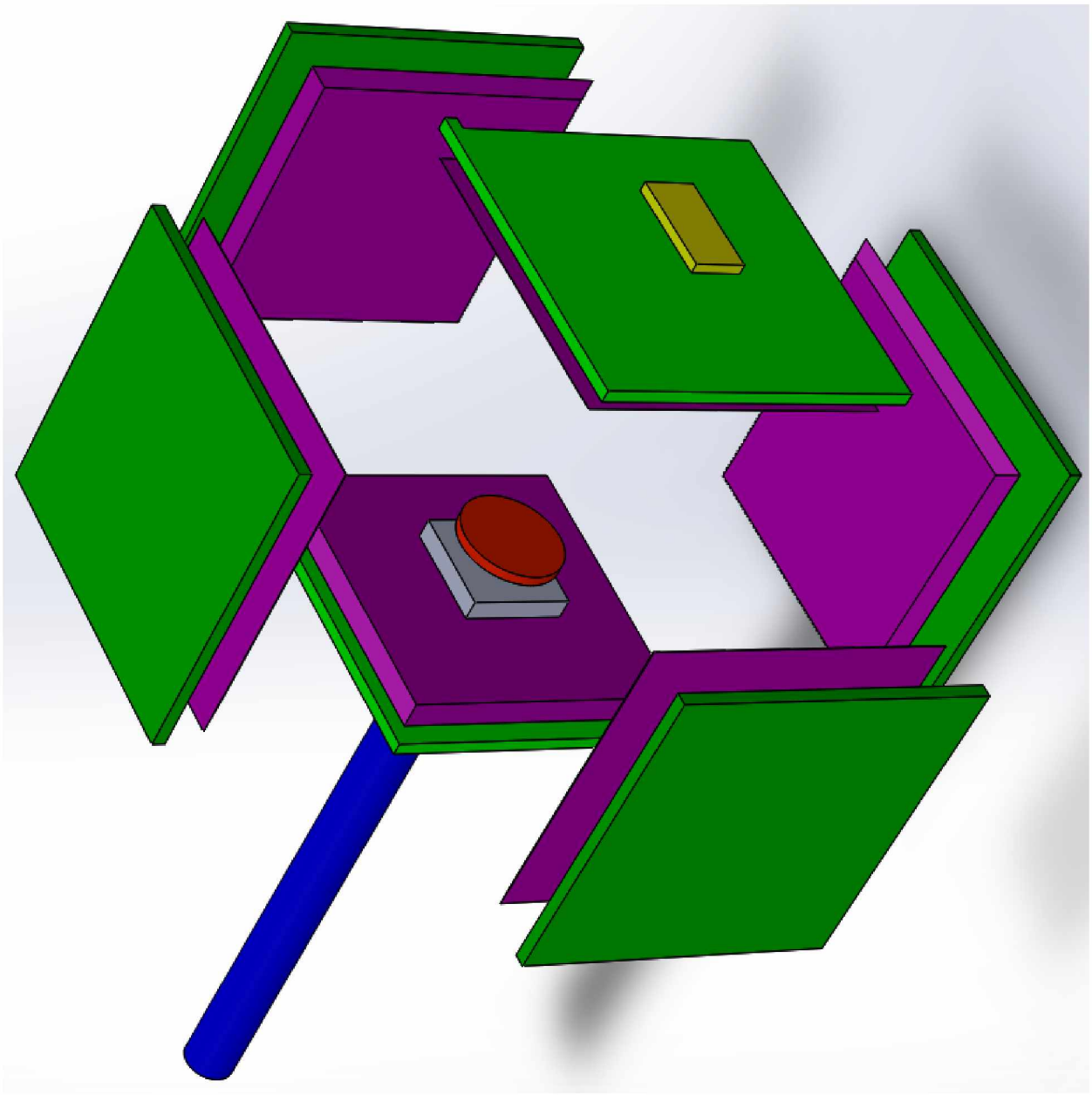

Figure 5.1: Solidworks model of the cubic reflective cavity design for the photofluorimeter. The green pieces are the aluminum plates, and the purple pieces represent the mirrors for reflecting light in the cavity.

## 5.2. Collimation of Light

This reflective cavity was used to detect a 1 milliMolar (mM) concentration fluorescence solution. However, the readings were all less than 50 in a range from 0-1023, which was much lower than expected.

To determine the causes of the low readings, a separate sample was run with one side of the aluminum plate removed from the cube, as shown in Figure 5.2. Figure 5.2(a) shows the cavity in use without the sample and light filter, while Figure 5.2(b) shows both. By comparing the images in Figure 5.2, a couple of conditions were observed: (1) there is a drastic difference in the color of light inside the cube with and without the sample, and (2) the level of green light emitted from the sample is fairly intensive. From this test it was concluded that the light was not collimating through the exit aperture in front of the light sensor. The non-collimated light reflecting across the inside of the cavity from one side to the opposite side is a function of the cube configuration. A significant loss of luminescent intensity occurs between two opposite sides within the reflective cavity as the photons lose energy when passing through any medium other than a vacuum.

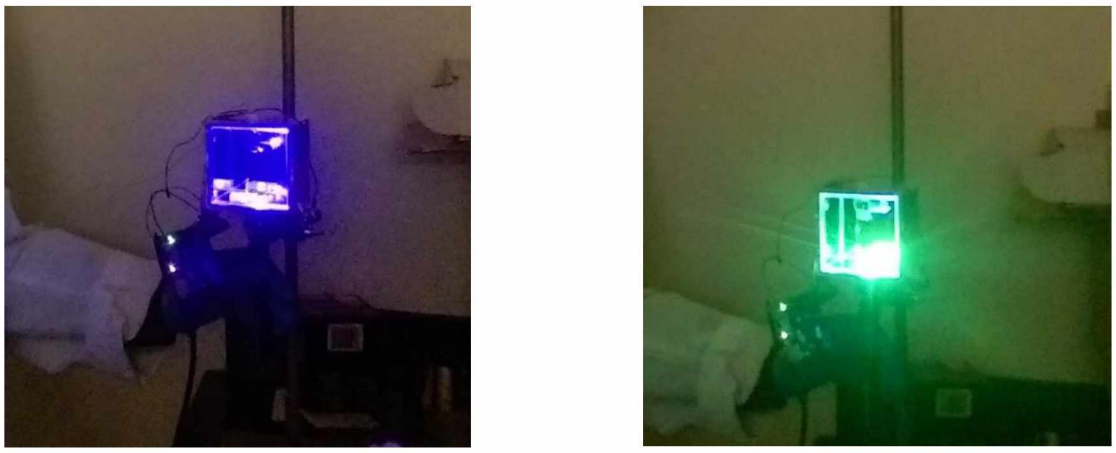

(a) (b)

Figure 5.2: Inside of the reflective cavity: (a) without sample and filter, and (b) with sample and filter.

A variety of collimation tools are available, including lenses, mirrors, and the Söller collimator. While each tool effectively collimates light from a multidirectional light source, the geometries of the reflective cavity and the need to maximize the transmission of photons from the sample to the light sensor suggest that a lens would be the most appropriate collimation tool. Ideally, this lens should be placed coaxially between the sample and the light sensor with a minimal distance between them. Due to time constraints, we tried an alternative method to resolve the light collimation problem: placing the light sensor inside the cubic cavity, thereby immersing the light sensor in the light emitted by the fluorophore. A schematic of this set-up is shown in Figure 5.3.

With the revised design in Figure 5.3, higher, more reasonable readings were produced from the same concentration levels. While reading these samples, it was observed that the 35 μL samples quickly get bleached by the intense source light from the laser. Keeping this in mind, the exposure time and therefore the number of consecutive readings needed to be limited.

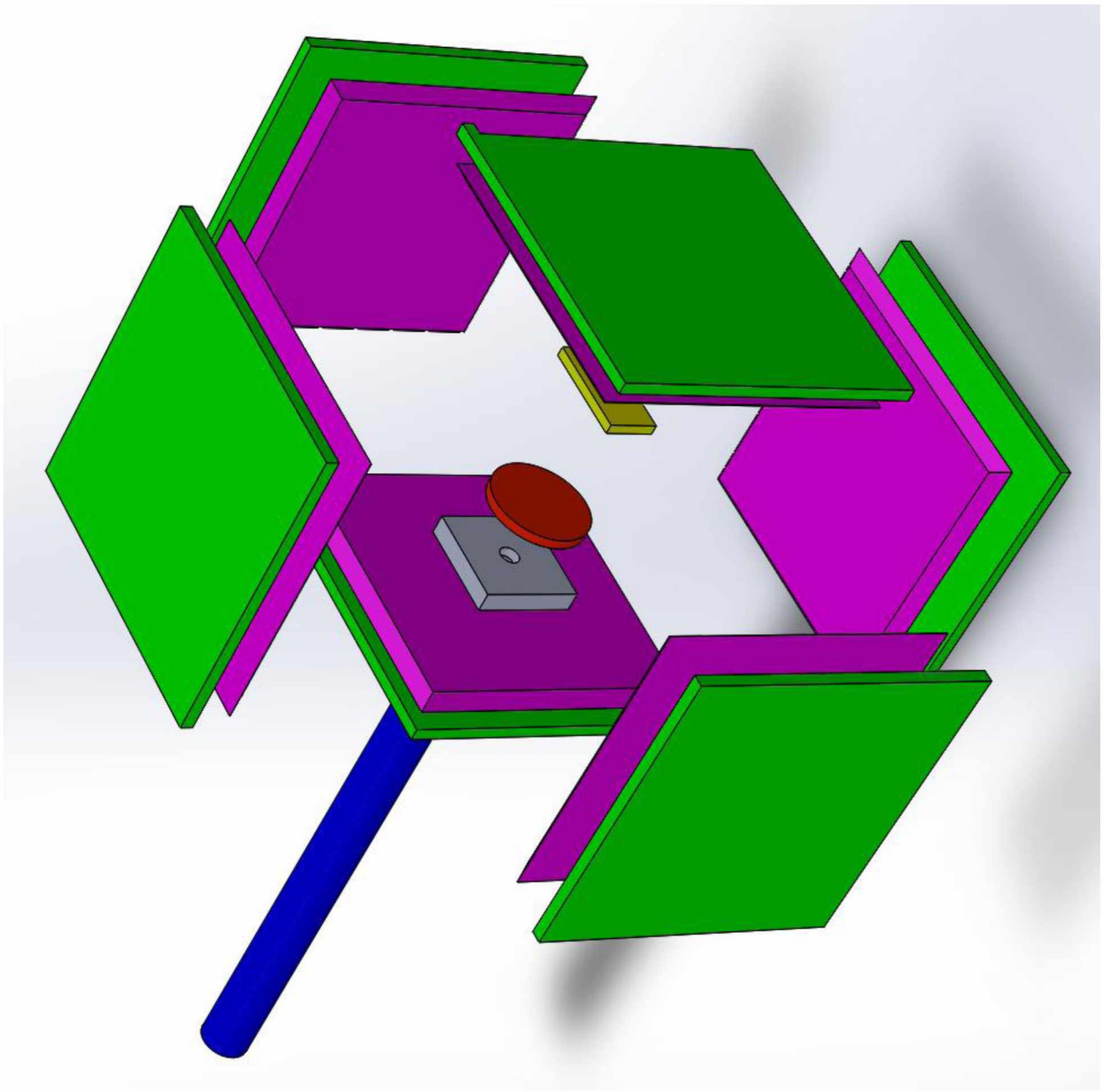

Figure 5.3: Final fluorimeter configuration.

## 5.3. Experiments

A set of ten fluorescein solutions, beginning at a concentration of 2mol/L and each diluted 10x from the previous sample, were prepared for testing. The objectives of testing are to prove the designed functionality of the reflective cavity and its detection limits with three experiments:

(1) Detectable range of fluorescein concentrations

(2) The possible lowest detectable concentration

(3) Detection of biological sample.

## 5.4. Results and Discussion

### 5.4.1. Concentration Range Finding for Fluorescein

The first set was a series of 10x diluted fluorescein solutions beginning at 2mol/L to generate a curve identifying the maximum and minimum detectable concentration levels for this configuration. The data for this set of samples can be seen in Table 5.1 and Figure 5.4. The green sample numbers represent the values given by the color sensor for the section of the photodiodes covered with green light filters, and the blue sample numbers represent the values given by the color sensor for the photodiodes covered with the blue light filters. The curve in Figure 5.4 shows that the reflective cavity is able to detect fluorescence concentrations between 0.2 μM and 2mM. The peak reading value occurs near the 2mM concentration and falls sharply with higher concentrations and more gradually with lower concentrations. This weighted bell curve shape may be caused by not having buffers to produce an optimal pH value in the water, since the maximum solubility of fluorescein is highly dependent on the pH of its solute.

Table 5.1: Green light and blue light readings from the photofluorimeter for various concentrations (C) of fluorescein samples.

| C (M)<br>Green Sample # | 2 | 0.2 | 0.02 | 0.002 | $2\times10^{-4}$ | $2\times10^{-5}$ | $2\times10^{-6}$ | $2\times10^{-7}$ | $2\times10^{-15}$ |
|---|---|---|---|---|---|---|---|---|---|
| 1 | 0 | 0 | 186 | 853 | 321 | 14 | 24 | 15 | 16 |
| 2 | 0 | 0 | 187 | 841 | 315 | 15 | 25 | 14 | 16 |
| 3 | 0 | 0 | 186 | 829 | 310 | 15 | 24 | 14 | 16 |
| 4 | 0 | 0 | 186 | 817 | 304 | 14 | 24 | 14 | 15 |
| 5 | 0 | 0 | 185 | 807 | 300 | 15 | 24 | 14 | 16 |
| 6 | 0 | 0 | 184 | 797 | 297 | 13 | 24 | 14 | 15 |
| 7 | 0 | 0 | 184 | 787 | 293 | 13 | 24 | 14 | 16 |
| 8 | 0 | 0 | 183 | 777 | 289 | 14 | 24 | 13 | 15 |
| 9 | 0 | 0 | 183 | 770 | 285 | 14 | 25 | 14 | 16 |
| 10 | 0 | 0 | 182 | 762 | 282 | 14 | 25 | 13 | 15 |
| average | 0 | 0 | 84.2 | 804 | 299.6 | 14.1 | 24.4 | 13.9 | 5.6 |

| C (M)<br>Blue Sample # | 2 | .2 | .02 | .002 | $2\times10^{-4}$ | $2\times10^{-5}$ | $2\times10^{-6}$ | $2\times10^{-7}$ | $2\times10^{-15}$ |
|---|---|---|---|---|---|---|---|---|---|
| 1 | 64 | 64 | 122 | 408 | 327 | 212 | 362 | 267 | 283 |
| 2 | 62 | 64 | 119 | 405 | 324 | 213 | 359 | 263 | 281 |
| 3 | 61 | 63 | 119 | 400 | 323 | 211 | 361 | 261 | 280 |
| 4 | 62 | 63 | 121 | 392 | 320 | 208 | 360 | 262 | 278 |
| 5 | 63 | 59 | 118 | 390 | 315 | 208 | 362 | 260 | 276 |
| 6 | 63 | 60 | 118 | 386 | 313 | 207 | 356 | 260 | 273 |
| 7 | 61 | 60 | 119 | 382 | 312 | 207 | 365 | 259 | 274 |
| 8 | 62 | 60 | 120 | 376 | 311 | 207 | 362 | 259 | 273 |
| 9 | 60 | 59 | 119 | 374 | 307 | 205 | 366 | 257 | 273 |
| 10 | 2 | 0 | 17 | 72 | 05 | 04 | 61 | 56 | 270 |
| average | 2 | 1.2 | 19.2 | 88.5 | 15.7 | 08.2 | 61.4 | 60.4 | 276.1 |

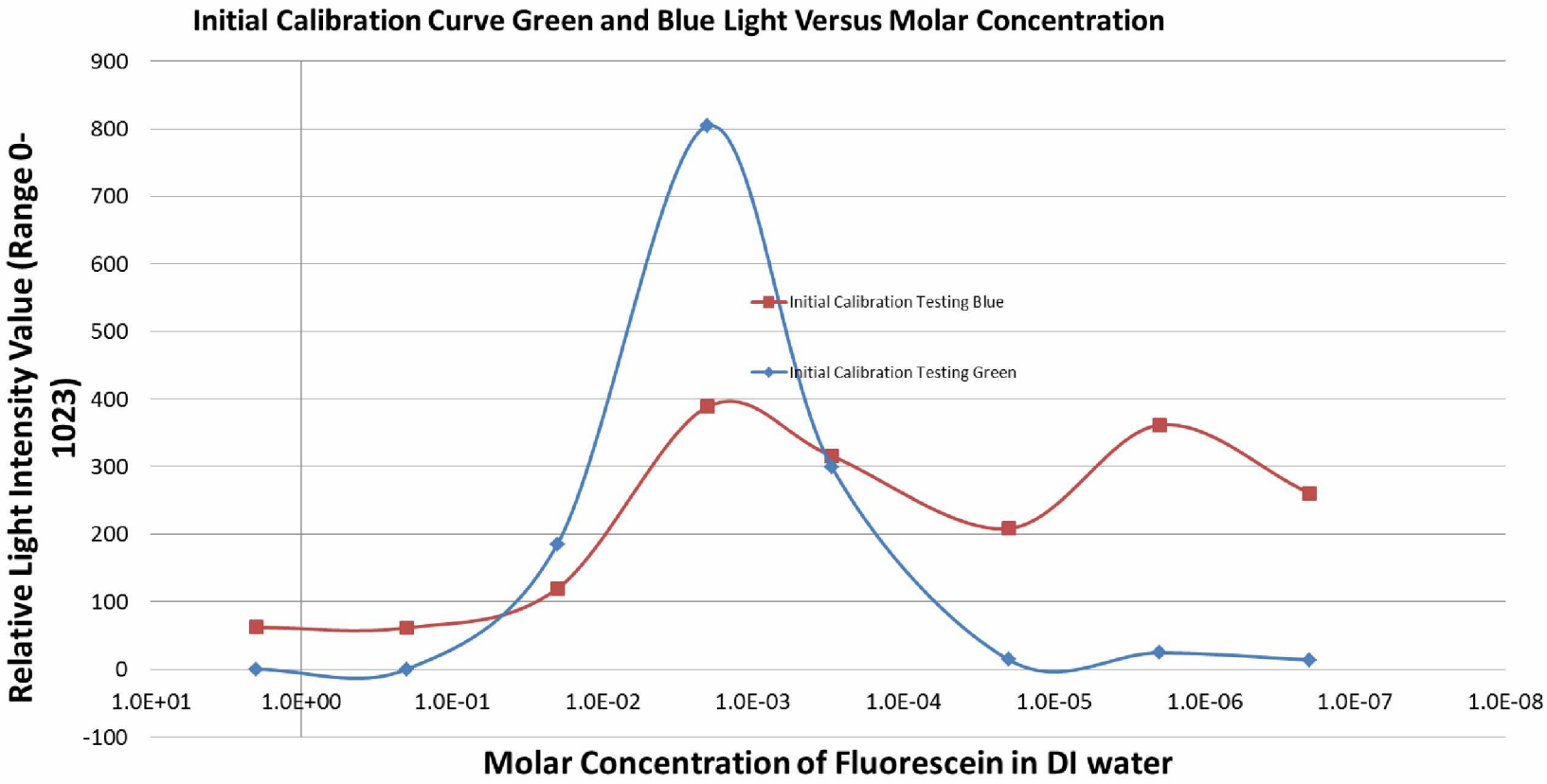


Figure 5.4: Graph of values read from the photofluorimeter output at descending concentrations beginning at a concentration of 2M.

### 5.4.2. Identifying the Optimal Fluorescence Concentration for Fluorescein

In order to pinpoint the fluorescein concentration with the highest emission levels when dissolved in unbuffered DI water, a second set of fluorescein samples was prepared by diluting stock solution with DI water. The solution concentrations used can be seen in Table 5.2. The results from this secondary test are shown in Table 5.2 and Figure 5.5.

The data from this series of tests shows that the values from samples of concentrations either higher or lower than 1mM are lower than the readings at 1mM. The concentrations lower than 1 mM generate a gradual slope of increasing readings with increasing concentration until the peak at 1 mM. The concentrations higher than 1 mM generate a steeper slope of increasing readings with increasing concentration. This is strong evidence that the optimal concentration for fluorescein in DI water is 1mM.

Table 5.2: Data obtained from incremental Fluorescein concentration testing between 1μM and 1mM.

| Con. (M) | 1 | 0.1 | 0.01 | 0.005 | 0.0025 | 0.00125 | 0.001 | 0.001 | $7.5\times10^{-4}$ | $5\times10^{-4}$ | $2.5\times10^{-4}$ | $1\times10^{-4}$ | $1\times10^{-4}$ | $1\times10^{-5}$ |
|---|---|---|---|---|---|---|---|---|---|---|---|---|---|---|
| Sample # | | | | | | | | | | | | | | |
| 1 | 0 | 0 | 186 | 423 | 614 | 774 | 853 | 878 | 811 | 781 | 666 | 291 | 321 | 14 |
| 2 | 0 | 0 | 187 | 420 | 608 | 764 | 841 | 858 | 793 | 765 | 653 | 285 | 315 | 15 |
| 3 | 0 | 0 | 186 | 417 | 601 | 752 | 829 | 841 | 775 | 747 | 640 | 280 | 310 | 15 |
| 4 | 0 | 0 | 186 | 415 | 595 | 743 | 817 | 825 | 760 | 732 | 628 | 276 | 304 | 14 |
| 5 | 0 | 0 | 185 | 413 | 593 | 734 | 807 | 809 | 743 | 717 | 617 | 272 | 300 | 15 |
| 6 | 0 | 0 | 184 | 410 | 587 | 724 | 797 | 794 | 729 | 704 | 609 | 268 | 297 | 13 |
| 7 | 0 | 0 | 184 | 408 | 583 | 716 | 787 | 781 | 716 | 690 | 599 | 265 | 293 | 13 |
| 8 | 0 | 0 | 183 | 406 | 579 | 707 | 777 | 768 | 702 | 679 | 592 | 262 | 289 | 14 |
| 9 | 0 | 0 | 183 | 403 | 576 | 700 | 770 | 756 | 691 | 668 | 582 | 259 | 285 | 14 |
| 10 | 0 | 0 | 182 | 403 | 571 | 694 | 762 | 745 | 679 | 657 | 576 | 257 | 282 | 14 |
| avg | 0 | 0 | 184.6 | 411.8 | 590.7 | 730.8 | 804 | 805.5 | 739.9 | 714 | 616.2 | 271.5 | 299.6 | 14.1 |

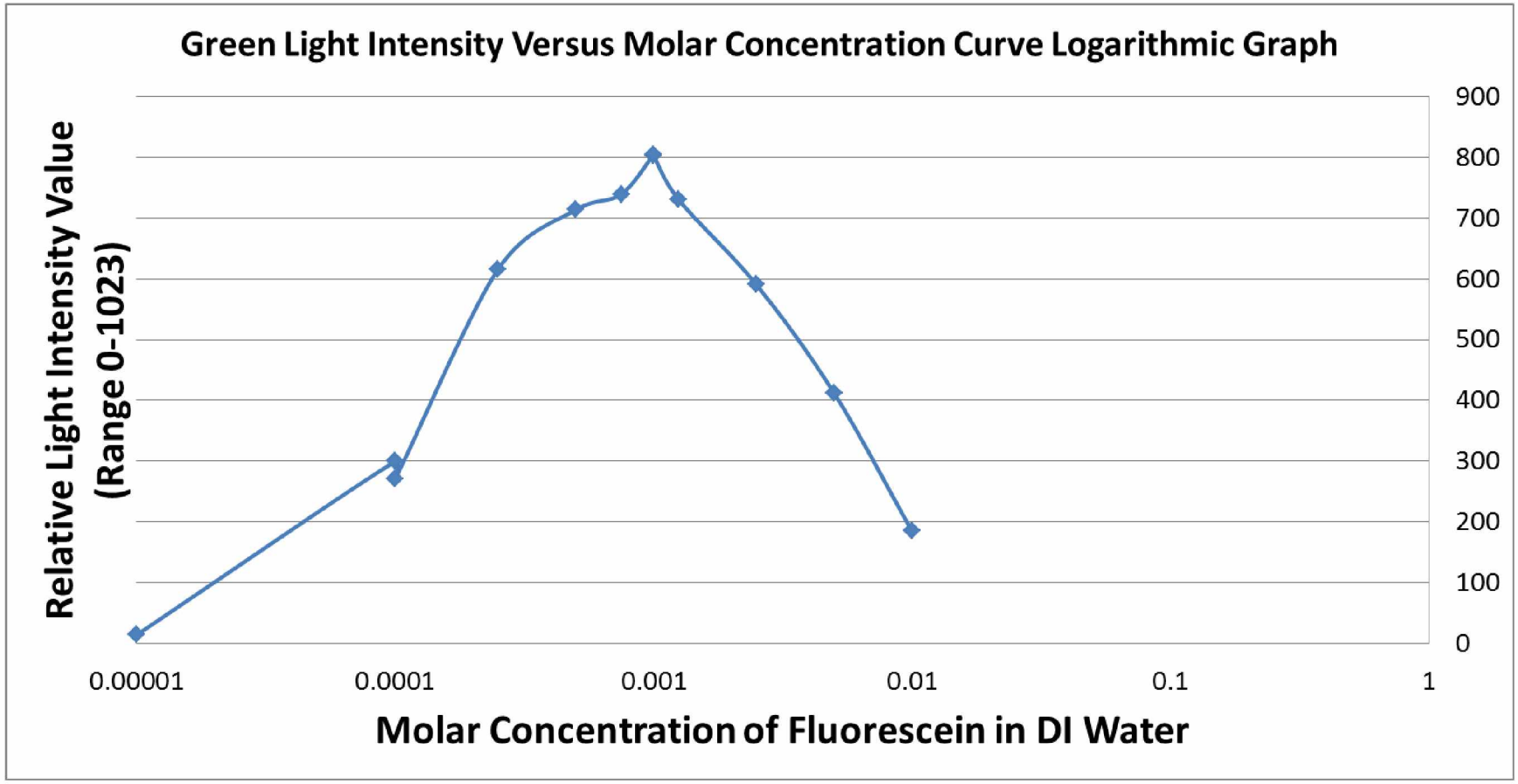


Figure 5.5: The range of fluorescein concentrations (between 1µM and 1mM) in which the reflective cavity can produce the maximum reading.

### 5.4.3. The Possible Lowest Detectable Concentration

Using the information obtained from the second series of tests, the range of concentrations to test was reduced to between 1mM and 1μM. As this photofluorimeter's purpose is the detection of chemicals in biological samples, the lowest detectable concentration is of more interest.

The third series of samples was produced using the 10x diluted solutions from the first set of data in this section and mixing them in 5 ml combinations of 1 ml increments. These solution concentrations give a resolution of about 3 points (on a scale of 0-1023) per 1μM concentration change for samples below 100μM and an average resolution of 2 points per μM change to produce a reference curve for fluorescein in DI water in the concentration range of [1 μM - 900 μM].

The data from this series of tests (in Table 5.3 and Figure 5.6) shows that the readings from the light sensor vs. the concentrations of samples form a continuous curve with a maximum intrasample standard deviation of 15.7 and an average intersample standard deviation of 8.5. These deviations (as compared to 1023, the maximum readout of the light sensor) indicate the consistency of the reflective cavity in assisting light reflection and focusing on the light sensor for detection. A linear region in the curve can be identified in the concentration range of [28 μM – 460 μM] on a logarithmic scale. The lowest detectable concentration for fluorescein in un-buffered DI water is about 1 μM.

Table 5.3: Data obtained from final set of fluorescein samples.

| | | Concentration (mM) | | | | | | | | | | | | | | | | | |
|---|---|---|---|---|---|---|---|---|---|---|---|---|---|---|---|---|---|---|---|
| Sample | Test# | 0 | $2\times10^{-3}$ | $4\times10^{-3}$ | $6\times10^{-3}$ | $8\times10^{-3}$ | 0.01 | 0.028 | 0.046 | 0.064 | 0.082 | 0.1 | 0.28 | 0.46 | 0.64 | 0.82 | 1 | 2.8 | 4.6 |
| 1 | 1 | 4 | 9 | 20 | 24 | 34 | 42 | 92 | 112 | 178 | 191 | 206 | 366 | 441 | 473 | 480 | 479 | 280 | 127 |
| | 2 | 4 | 9 | 20 | 23 | 34 | 42 | 91 | 111 | 175 | 187 | 202 | 360 | 432 | 465 | 474 | 473 | 277 | 128 |
| | 3 | 4 | 9 | 20 | 23 | 33 | 43 | 89 | 109 | 169 | 182 | 198 | 350 | 424 | 458 | 466 | 465 | 275 | 128 |
| | 4 | 3 | 8 | 20 | 22 | 33 | 41 | 87 | 106 | 169 | 178 | 192 | 342 | 415 | 449 | 460 | 458 | 272 | 128 |
| | 5 | 3 | 8 | 20 | 21 | 32 | 41 | 86 | 105 | 163 | 174 | 188 | 335 | 407 | 443 | 455 | 450 | 270 | 127 |
| | Avg | 3.6 | 8.6 | 20 | 22.6 | 33.2 | 41.8 | 89 | 108.6 | 170.8 | 182.4 | 197.2 | 350.6 | 423.8 | 457.6 | 467 | 465 | 274.8 | 127.6 |
| 2 | 1 | 7 | 11 | 16 | 26 | 33 | 42 | 80 | 118 | 168 | 195 | 219 | 376 | 474 | 463 | 476 | 483 | 255 | 131 |
| | 2 | 7 | 13 | 15 | 25 | 33 | 40 | 79 | 117 | 169 | 192 | 213 | 369 | 467 | 458 | 473 | 478 | 255 | 131 |
| | 3 | 7 | 12 | 16 | 26 | 32 | 40 | 78 | 114 | 163 | 187 | 207 | 358 | 459 | 448 | 465 | 471 | 254 | 131 |
| | 4 | 7 | 11 | 16 | 26 | 32 | 39 | 75 | 113 | 159 | 183 | 201 | 349 | 448 | 442 | 458 | 463 | 252 | 131 |
| | 5 | 6 | 11 | 16 | 25 | 32 | 40 | 74 | 109 | 156 | 179 | 197 | 340 | 440 | 434 | 450 | 456 | 249 | 128 |
| | Avg | 6.8 | 11.6 | 15.8 | 25.6 | 32.4 | 40.2 | 77.2 | 114.2 | 163 | 187.2 | 207.4 | 358.4 | 457.6 | 449 | 464.4 | 470.2 | 253 | 130.4 |
| 3 | 1 | 5 | 14 | 19 | 24 | 29 | 40 | 65 | 119 | 190 | 174 | 184 | 402 | 421 | 476 | 458 | 465 | 256 | 151 |
| | 2 | 6 | 13 | 19 | 24 | 29 | 39 | 66 | 118 | 186 | 174 | 180 | 397 | 422 | 469 | 462 | 457 | 258 | 152 |
| | 3 | 4 | 14 | 19 | 23 | 28 | 38 | 65 | 116 | 183 | 170 | 176 | 387 | 415 | 461 | 454 | 451 | 255 | 152 |
| | 4 | 5 | 15 | 19 | 23 | 29 | 39 | 64 | 114 | 179 | 165 | 172 | 378 | 406 | 453 | 449 | 445 | 253 | 151 |
| | 5 | 4 | 13 | 19 | 23 | 28 | 38 | 63 | 111 | 175 | 161 | 167 | 369 | 398 | 446 | 441 | 438 | 251 | 150 |
| | Avg | 4.8 | 13.8 | 19 | 23.4 | 28.6 | 38.8 | 64.6 | 115.6 | 182.6 | 168.8 | 175.8 | 386.6 | 412.4 | 461 | 452.8 | 451.2 | 254.6 | 151.2 |
| 4 | 1 | 5 | 12 | 16 | 26 | 34 | 39 | 67 | 121 | 161 | 186 | 216 | 364 | 442 | 493 | 461 | 480 | 264 | 136 |
| | 2 | 5 | 12 | 16 | 26 | 32 | 39 | 66 | 120 | 160 | 183 | 211 | 356 | 434 | 486 | 458 | 473 | 262 | 140 |
| | 3 | 4 | 11 | 16 | 25 | 32 | 38 | 66 | 117 | 157 | 177 | 205 | 347 | 423 | 477 | 450 | 465 | 260 | 139 |
| | 4 | 5 | 12 | 15 | 26 | 33 | 37 | 64 | 115 | 153 | 172 | 201 | 339 | 415 | 469 | 442 | 459 | 258 | 137 |
| | 5 | 4 | 13 | 16 | 25 | 33 | 37 | 63 | 112 | 150 | 168 | 194 | 333 | 406 | 461 | 435 | 452 | 256 | 137 |
| | Avg | 4.6 | 12 | 15.8 | 25.6 | 32.8 | 38 | 65.2 | 117 | 156.2 | 177.2 | 205.4 | 347.8 | 424 | 477.2 | 449.2 | 465.8 | 260 | 137.8 |
| 5 | 1 | 5 | 13 | 21 | 23 | 35 | 39 | 87 | 143 | 158 | 190 | 217 | 369 | 429 | 453 | 476 | 453 | 270 | 138 |
| | 2 | 6 | 12 | 20 | 23 | 35 | 38 | 86 | 142 | 155 | 187 | 210 | 363 | 425 | 450 | 474 | 447 | 271 | 139 |
| | 3 | 6 | 13 | 21 | 22 | 35 | 39 | 85 | 138 | 152 | 182 | 204 | 353 | 415 | 443 | 470 | 439 | 268 | 138 |
| | 4 | 5 | 12 | 20 | 22 | 34 | 38 | 82 | 135 | 148 | 178 | 199 | 345 | 405 | 433 | 464 | 433 | 266 | 139 |
| | 5 | 6 | 13 | 20 | 23 | 34 | 38 | 82 | 133 | 145 | 173 | 194 | 338 | 396 | 424 | 457 | 427 | 264 | 137 |
| | Avg. | 5.6 | 12.6 | 20.4 | 22.6 | 34.6 | 38.4 | 84.4 | 138.2 | 151.6 | 182 | 204.8 | 353.6 | 414 | 440.6 | 468.2 | 439.8 | 267.8 | 138.2 |
| Avg reading | | 5.1 | 11.7 | 18.2 | 24.0 | 32.3 | 39.4 | 76.08 | 118.7 | 164.8 | 179.5 | 198.1 | 359.4 | 426.4 | 457.1 | 460.3 | 458.4 | 262.0 | 137.0 |

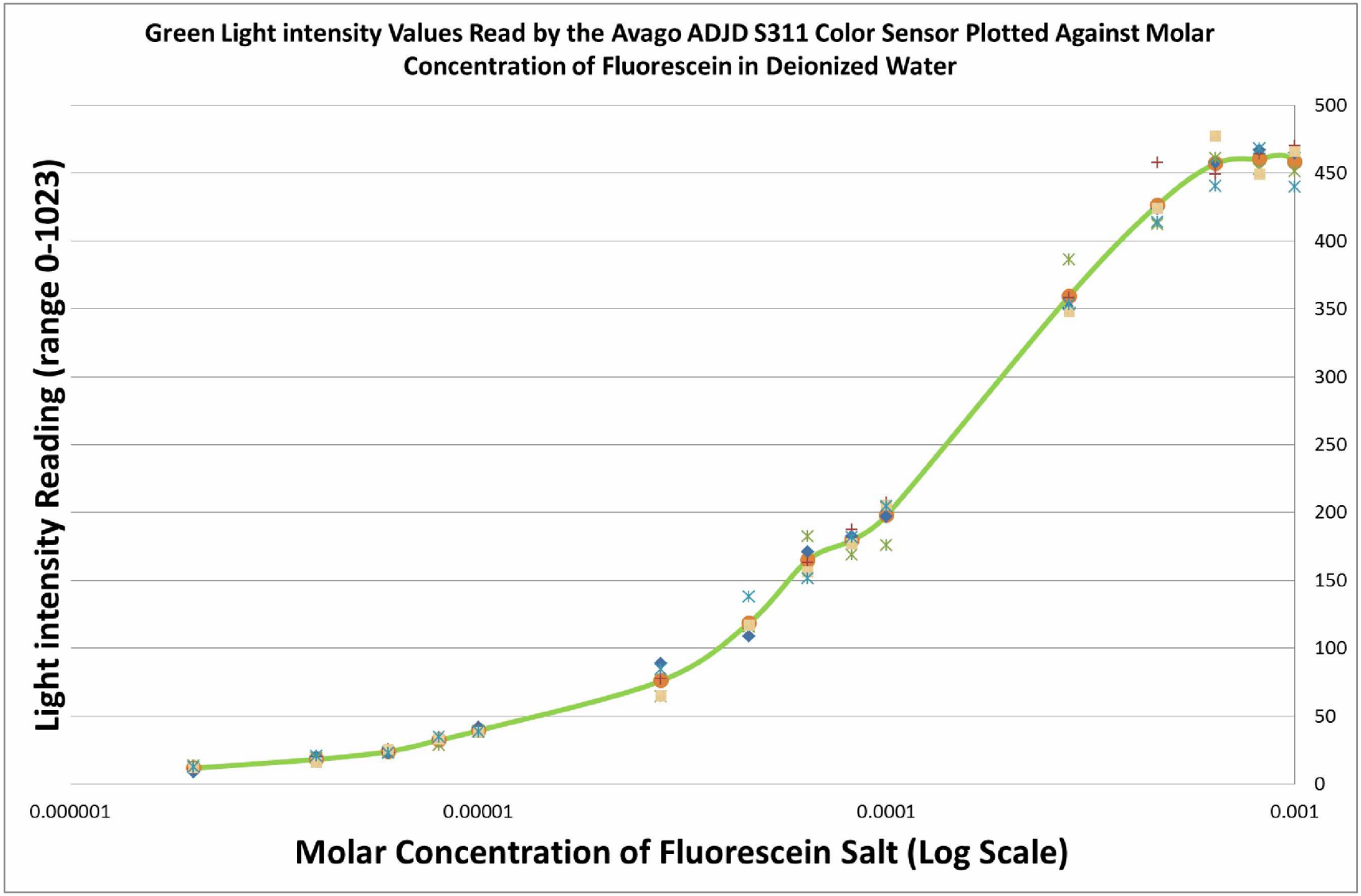


Figure 5.6: Calibration curve generated using the cubic reflective cavity fluorimeter.

### 5.4.4. Stage 4 Detection of Biological Sample

With sufficient evidence that the photofluorimeter was working properly, the final experiment was to test its applicability for detecting a biologically relevant chemical, D-Glutamic acid. D-Glutamic acid is an amino acid occurring naturally in the human body; abnormal levels are associated with schizophrenia [32]. In order to measure the concentration of D-Glutamic acid by way of fluorescence detection, NDA (2,3-naphthalenedicarboxaldhyde) was used to bind with the glutamic acid. NDA has an emission wavelength of 480-490 nm when excited with 420 nm light [7, 33].

It is worth noting that the previous series of tests were carried out using non-buffered DI water, and the precision of the sample fluid concentrations was constrained by the scale accuracy (as rough as 0.01 g) and the production of designated solution volumes by manual syringes. In contrast, this test was carried out using pipettes for precise volume measurements, buffered milli-Q type 1 water, and a scale accurate to 0.0001 grams.

The data obtained from the D-Glutamate test set are shown in Table 5.4 and Figure 5.6. From this set of data, several things are immediately apparent. Chief among these is that the readings of the buffered milli-Q water control test were zero and the fact that the readings are linear in nature on a log scale graph. These observations indicate that the results from the previous tests are only useful as proof of concept.

Table 5.4: Data obtained from D-Glutamate and NDA testing.

| | | Concentration (μM) | | | | | |
|---|---|---|---|---|---|---|---|
| Sample # | Test # | 0 | 0.574 | 2.87 | 5.74 | 28.7 | 57.4 |
| 1 | 1 | 0 | 0 | 0 | 1 | 29 | 63 |
| | 2 | 0 | 0 | 0 | 1 | 28 | 61 |
| | 3 | 0 | 0 | 0 | 1 | 27 | 59 |
| | 4 | 0 | 0 | 0 | 0 | 27 | 57 |
| | 5 | 0 | 0 | 0 | 1 | 24 | 55 |
| | Avg | 0 | 0 | 0 | 0.8 | 27 | 59 |
| 2 | 1 | 0 | 0 | 0 | 1 | 30 | 62 |
| | 2 | 0 | 0 | 0 | 1 | 29 | 60 |
| | 3 | 0 | 0 | 0 | 0 | 26 | 59 |
| | 4 | 0 | 0 | 0 | 0 | 25 | 56 |
| | 5 | 0 | 0 | 0 | 0 | 23 | 55 |
| | Avg | 0 | 0 | 0 | 0.4 | 26.6 | 58.4 |
| 3 | 1 | 0 | 0 | 0 | 3 | 30 | 59 |
| | 2 | 0 | 0 | 0 | 3 | 29 | 59 |
| | 3 | 0 | 0 | 0 | 3 | 28 | 57 |
| | 4 | 0 | 0 | 0 | 3 | 28 | 55 |
| | 5 | 0 | 0 | 0 | 3 | 26 | 53 |
| | Avg | 0 | 0 | 0 | 3 | 28.2 | 56.6 |
| 4 | 1 | 0 | 0 | 0 | 2 | 28 | 63 |
| | 2 | 0 | 0 | 0 | 1 | 29 | 60 |
| | 3 | 0 | 0 | 0 | 2 | 27 | 58 |
| | 4 | 0 | 0 | 0 | 2 | 26 | 54 |
| | 5 | 0 | 0 | 0 | 1 | 25 | 54 |
| | Avg | 0 | 0 | 0 | 1.6 | 27 | 57.8 |
| 5 | 1 | 0 | 0 | 0 | 1 | 27 | 61 |
| | 2 | 0 | 0 | 0 | 2 | 26 | 58 |
| | 3 | 0 | 0 | 0 | 2 | 26 | 58 |
| | 4 | 0 | 0 | 0 | 2 | 24 | 55 |
| | 5 | 0 | 0 | 0 | 1 | 23 | 53 |
| | Avg | 0 | 0 | 0 | 1.6 | 25.2 | 57 |
| Sample Average | | 0 | 0 | 0 | 1.48 | 26.8 | 57.76 |

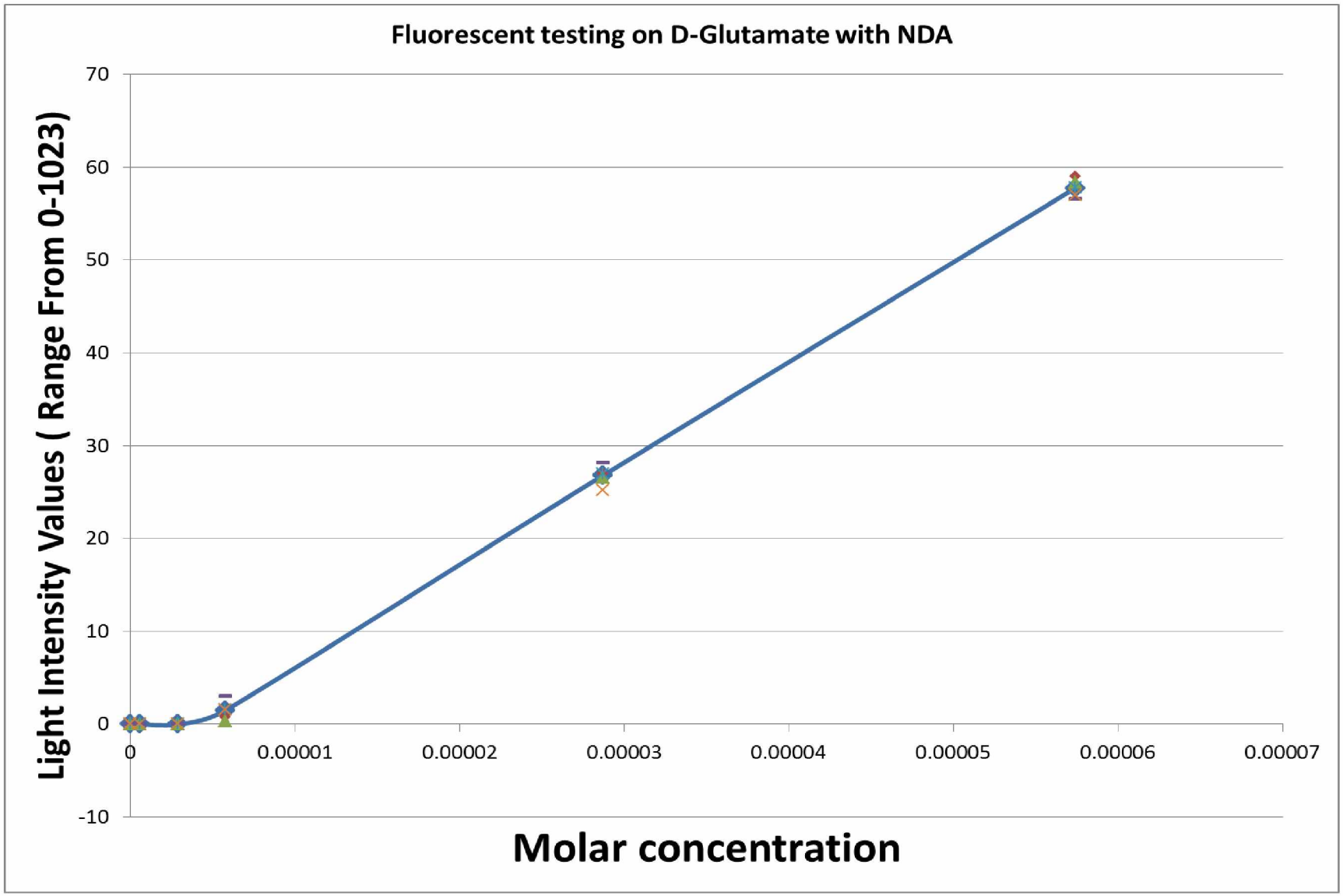


Figure 5.7: D-glutamate test results.

From the information presented in Table 5.4 and Figure 5.7, it is apparent that the lowest detectable concentration for this device is about 5 µM when using D-Glutamate tagged with the NDA fluorescent marker. The data also shows a resolution of 1 point for every µM change in concentration, with an extremely low and consistent standard deviation at the value of 1. As mentioned before, the peak emission wavelength of the NDA fluorophore is 490 nm, which is below the pass band parameters of the light filter. The graph in Figure 5.8 shows the excitation spectrum of NDA-labeled amino acid (curve 1) and the emission spectrum of the NDA-labeled amino acid (curve 2). The emission spectrum shown indicates that although the peak intensity occurs below 500 nm, a large portion of the emitted light is capable of passing through the filter.

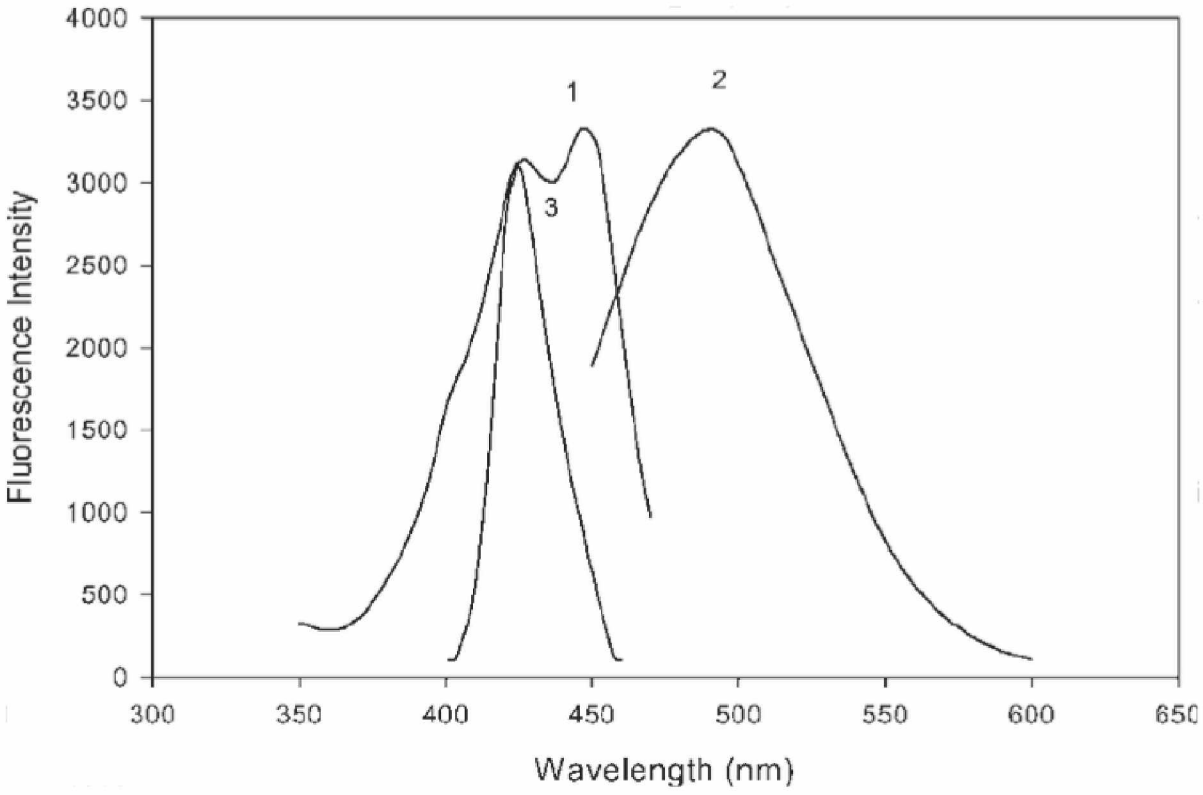


Figure 5.8: Spectra of the excitation (label-1) and emission (label-2) of NDA labeled amino acids [34].

# Chapter 6. Conclusions and Future Work

## 6.1. Conclusions

The experimental data from the D-Glutamate tests, shown graphically in Figure 5.6 and Figure 5.7, exhibit two features: (1) they show a linear relationship between the intensity of emitted fluorescent light and the concentration of D-Glutamate on a logarithmic scale, and (2) they show a very small deviation from each other. These tests have proven that this photofluorimeter can effectively detect the presence and determine the concentration of a variety of photofluorophores.

Although the lowest detectable concentration for this particular photofluorimeter is on the order of 1μM for fluorescein or NDA labeled D-Glutamate, it is worth noting that it was crudely constructed and cost less than $300 altogether. This photofluorimeter can be improved in the future with a more sensitive light sensor, multiple light filters, and a spherical reflective cavity to reach a detection sensitivity at the order of 1 nM or smaller.

Through this thesis work, a portable, field-use photofluorimeter has been produced. This new tool is capable of interpreting fluorescence samples produced from microfluidics chip labs integrated in-situ where sustained power sources are unavailable. Including this photofluorimeter, along with a variety of microfluidics chips, in the standard equipment of emergency medical staff could provide a variety of diagnoses within minutes with only a few drops of blood. These early diagnoses could be the determining factor for survival for many patients.

## 6.2. Future Development

For future development, the lowest detectable concentration for this photofluorimeter could be improved by several orders of magnitude by reducing the size and changing the shape of the reflective cavity to a sphere and installing a light sensor with better resolution and filters.

The apparatus will also require a chip tray which will allow the user to simply place the specimen tray into the reflective cavity. Because the intent of this photofluorimeter is to be a general use photospectrofluorimeter for microfluidics chips, the chip will require inlet and outlet channels to allow fluids to flow through the system. In order to become a complete stand-alone device, it will also require a battery pack (at the 5V level) and a low power visual display for the results. In order to increase the variety of usable fluorescent markers, electrical nodes for electrochemoluminescence may also be incorporated into the chip and chip tray. A solid works rendering of the enhanced fluorimeter is shown in Figure 6.1.

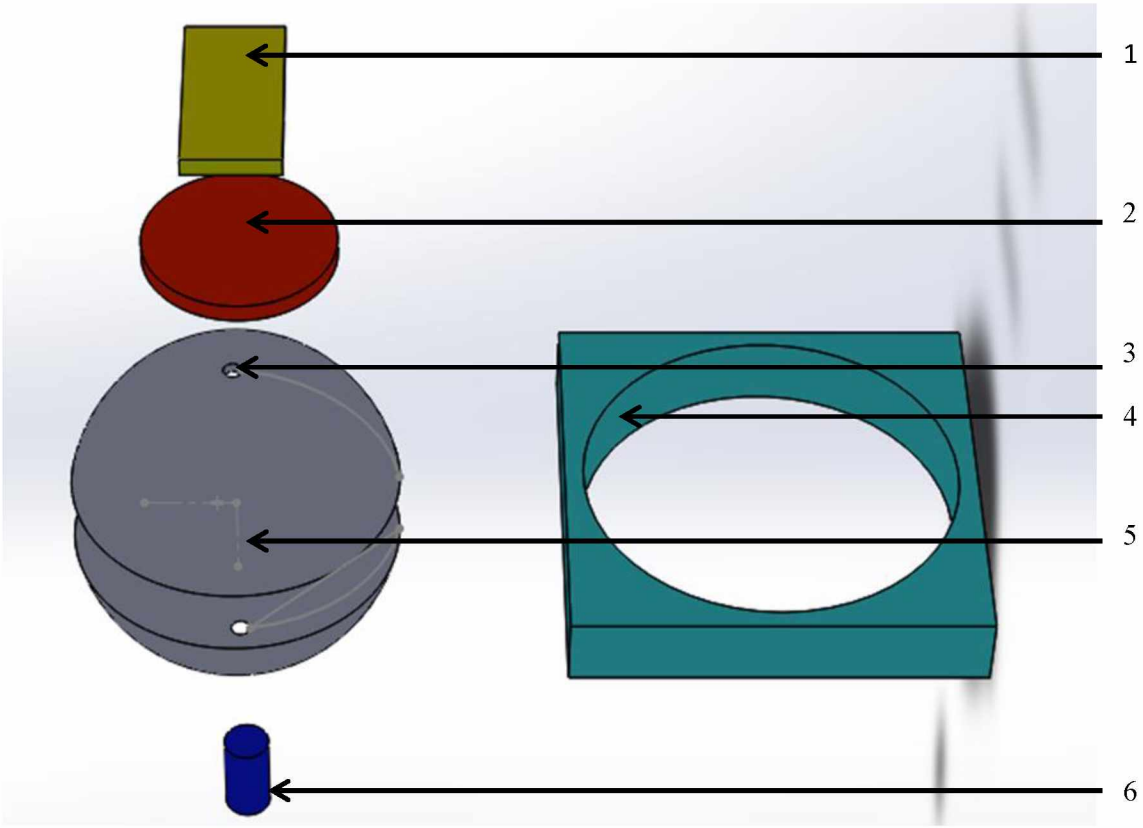


Figure 6.1: SolidWorks model of the spherical reflective cavity design for the photofluorimeter. The yellow piece (1) is the light sensor, the red piece (2) is the fluorescence light filter, the white circles on the grey pieces (3) are light inlet and outlet apertures, the teal piece (4) is the sample chip tray, the grey hemispheres (5) make up the spherical cavity with reflective interior, and the blue cylinder (6) is the small LED laser light source with excitation light filter.

Because this fluorimeter is designed to be one module connected to other microfluidic chips, the capabilities of the fluorimeter can be greatly expanded simply by providing a variety of microfluidic chips. A versatile ELISA assay chip is proposed for analyzing bodily fluids.

This ELISA assay chip was designed in two modules for compatibility with the fluorimeter. Module 1 was designed to contain and prepare a sample which has already been separated from whole blood [35, 36]. This module includes inputs for cell care, fluids growth medium, and saline, and one for the protein marker fluid as well as outlets for waste and transport to module 2. Module 2 was designed primarily as a sample container and observation platform. It contains a circulation pump to continuously move the labeled sample fluid over the ELISA platform, which is a region of the microfluidics chip containing a large amount of surface area that has been coated with monoclonal capture antibodies. As the labeled sample fluid flows over the capture antibodies, the analyte of interest binds to the capture antibody applied to the surface of the ELISA platform. Modules 1 and 2 contain a microscale circulation pump to facilitate adequate chemical reaction. Schematic designs of modules 1 and 2 are shown in Figure 6.2.

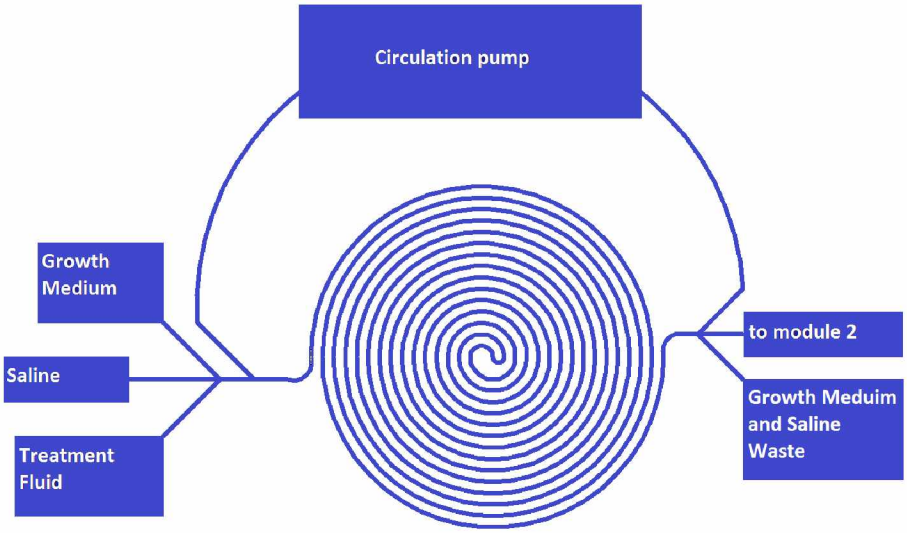


(a) Module 1

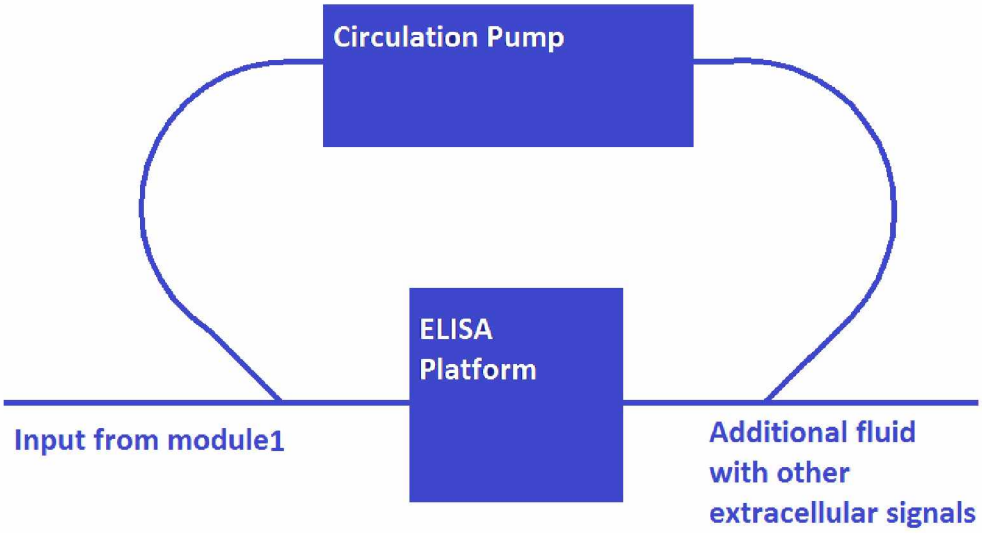


(b) Module 2

Figure 6.2: Microfluidics chip modular design. (a) Module 1 includes growth medium, saline and marker antibodies for the ELISA assay as well as a circulation pump and drainage outlet for waste and transport to the second module. (b) Module 2 contains a micro well ELISA platform for analyte capture and detection.

The detection apparatus was designed to work using the ELISA platform shown in Figure 6.2 (b) as the analysis chamber where the analyte of interest will be bound. In order to properly design a detection apparatus, an in-depth investigation into the ELISA assay technology is needed. Research using direct communication with scientists from various biological supply companies [37-41] revealed that standard ELISA assays provide colorimetric results which require image processing software to determine concentration. Upon further investigation, it was discovered that fluorescence could be a solution to concentration detection as well as miniaturization. Although the majority of ELISA assays use colorimetric markers, fluorescent markers are also available.

A portable photospectrofluorimeter could be useful in many applications including but not limited to ecological testing, cancer research and detection, viral and bacterial detection, and drug testing. This photofluorimeter is a stand-alone, portable, and inexpensive analysis tool which provides results in less than 30 minutes. It can be used to read the results of a variety of LOC technologies directly, which would eliminate the requirement for proprietary software or hardware to read the fluorometric results of each chip.

# References


[1] Whitesides, G. M., 2006, "The origins and the future of microfluidics," Nature, 442(7101), pp. 368-373.

[2] Kuznetsov, I. A., 2011, "Microfluidics: Theory and applications." Nova Science Publishers.

[3] Chen, C.-F., 2010, "Constitutive Law for Miniaturized Quantitative Microdialysis," 26th Souther Biomedical Engineering Conference, International Federation for Medical and Biological Engineering, College Park Maryland, pp. 77-80.

[4] Cleave, J. V., 2015, "Fluorescence Vs. Phosphorescence," http://scienceprojectideasforkids.com/wp-content/uploads/2010/06/fluorescence-excited-electron.jpg.

[5] Bixler, J. N., Cone, M. T., Hokr, B. H., Mason, J. D., Figueroa, E., Fry, E. S., Yakovlev, V. V., and Scully, M. O., 2014, "Ultrasensitive detection of waste products in water using fluorescence emission cavity-enhanced spectroscopy," Proceedings of the National Academy of Sciences, 111(20), pp. 7208-7211.

[6] Chin, C. D., Laksanasopin, T., Cheung, Y. K., Steinmiller, D., Linder, V., Parsa, H., Wang, J., Moore, H., Rouse, R., Umviligihozo, G., Karita, E., Mwambarangwe, L., Braunstein, S. L., van de Wijgert, J., Sahabo, R., Justman, J. E., El-Sadr, W., and Sia, S. K., 2011, "Microfluidics-based diagnostics of infectious diseases in the developing world," Natural Medicine, 17(8), pp. 1015-1019.

[7] Frerichs, V. A., Herrmann, J. K., Aguirre, A., and Colón, L. A., 2004, "Trace level determination of substance P using capillary electrophoresis and laser-induced fluorescence," Microchemical Journal, 78(2), pp. 135-142.

[8] Iles, R., 2012, "What will be the Future Development of Electrochemical Biosensors for the Detection and Quantification of Biomarkers?," Journal of Bioengineering and Biomedical Science.

[9] Gervais, L., and Delamarche, E., 2009, "Toward one-step point-of-care immunodiagnostics using capillary-driven microfluidics and PDMS substrates," Lab on a Chip, 9(23), pp. 3330-3337.

[10] Sista, R. S., Eckhardt, A. E., Wang, T., Graham, C., Rouse, J. L., Norton, S. M., Srinivasan, V., Pollack, M. G., Tolun, A. A., Bali, D., Millington, D. S., Pamula, V. K., 2011, "Digital Microfluidic Platform for Multiplexing Enzyme Assays: Impl," Clinical Chemestry, 57(10), p. 8.

[11] Sia, S., 2015, "Smartphone, Finger Prick, 15 Minutes, Diagnosis—Done!," http://engineering.columbia.edu/smartphone-finger-prick-15-minutes-diagnosis%E2%80%94done-0.

[12] Yu, H., Tan, Y., and Cunningham, B. T., 2014, "Smartphone Fluorescence Spectroscopy," Analytical Chemistry, 86(17), pp. 8805-8813.

[13] Stroud, M. H., Prodhan, P., Moss, M. M., and Anand, K. J. S., 2008, "Redefining the golden hour in pediatric transport," Pediatric Critical Care Medicine, 9(4), pp. 435-437.

[14] Waltz Mess- und Regeltechnik, 2015, "PAM-2500 chloyophyll fluorometer." http://www.walz.com/products/chl_p700/pam-2500/introduction.html

[15] Jovanovich, S., Nielsen, W. D., Cohen, D. S., Reknor, M., Vangbo, M., Gelder E. V., Majlof, L., El-Sissi, O., 2011, "US patent NO. US 2011/0005932 A1 Universal sample preparation system and use in an integrated analysis system."

[16] Silverbrook, M. A. K., 2011, "US patent NO. US 2011/0312622 A1 Microfluidic device with low-volume hybridization chambers for electrochemiluminescent detection of target sequences."

[17] Suzuki, Y., 2009, "US patent NO. US 2009/0189087 A1 Measuring device and measuring method."

[18] So, P. T., Chen,Y. D., 2001, "Fluorescence spectrophotometry," Encyclopedia of Life Sciences, Wiley and Sons, Wiley Online Library.

[19] Fry, E. S., Musser, J., Kattawar, G. W., and Zhai, P.-W., 2006, "Integrating cavities: temporal response," Applied Optics, 45(36), pp. 9053-9065.

[20] Microsystems, L., 2008, "Quantitative Fluorescence," http://www.leica-microsystems.com/science-lab/topics/quantitative-fluorescence/topic/Topic///pagetype_t/abstract/.

[21] Gaigalas, A. K., Wang, L., 2008, "Measurement of the Fluorescence Quantum Yield Using a Spectrometer With an Integrating Sphere Detector," Journal of Research of the National Institute of Standards and Technology, 113(1), p. 12.

[22] Godfrey, L. , 1997, "Choosing the Detector for your Unique Light Sensing Application," EG&G Optoelectronics http://www.johnloomis.org/ece445/topics/egginc/tp4.html.

[23] Clive TEC, "Diodes," http://clivetec.0catch.com/Diodes.html#Avalanche.

[24] iBizware Solutions, 2011, "How a Digital Camera Works," http://www.shortcourses.com/guide/guide1-3.html.

[25] ThorLabs.com, 2015, "FBH520-40 - Premium Bandpass Filter, Ø25 mm, CWL = 520 nm, FWHM = 40 nm ", http://www.thorlabs.us/thorproduct.cfm?partnumber=FBH520-40.

[26] Augarten, S., 1974, "The Most Widely Used Computer on a Chip", Smithsonian database. http://smithsonianchips.si.edu/augarten/p38.htm

[27] Sparkfun, 2011, "Avago ADJD S311-CR999 Color Light Sensor," https://www.sparkfun.com/products/retired/10656

[28] Aldrich, S., 2015, "Fluorescein sodium salt," http://www.sigmaaldrich.com/catalog/product/sial/f6377?lang=en&region=US.

[29] Chen, C., and Bender, C., 2015, "PDMS-PDMS bonding by air plasma," in preparation.

[30] Rich Watkins, J. V., 2008, "Rayleigh Scattering," http://home.comcast.net/~vinelandrobotics/.

[31] Jones, R. V., 2000, "V. Elementary Laser Models," http://people.seas.harvard.edu/~jones/ap216/lectures/ls_2/ls2_u5/ls2_unit_5.html.

[32] Hashimoto, K., Fukushima, T., Shimizu, E., Komatsu, N., Watanabe, H., Shinoda, N., Nakazato, M., Kumakiri, C., Okada, S., Hasegawa, H., Imai, K., and Iyo, M., 2003, "Decreased serum levels of D-serine in patients with schizophrenia: evidence in support of the N-methyl-D-aspartate receptor hypofunction hypothesis of schizophrenia," Archives of general psychiatry, 60(6), pp. 572-576.

[33] Aldrich, S., 2015, "NDA," http://www.sigmaaldrich.com/catalog/product/sigma/70215?lang=en&region=US.

[34] Zhao, S., H. and Xiao, D., 2006, "Optical fiber light-emitting diode-dinuced fluorescence detection for capillary electrophoresis," Electrophoresis , (27), pp. 461-467.

[35] Songjaroen, T., Dungchai, W., Chailapakul, O., Henry, C. S., and Laiwattanapaisal, W., 2012, "Blood separation on microfluidic paper-based analytical devices," Lab on a Chip, 12(18), pp. 3392-3398.

[36] Yang, S., Undar, A., and Zahn, J. D., 2006, "A microfluidic device for continuous, real time blood plasma separation," Lab on a Chip, 6(7), pp. 871-880.

[37] Abcam, 2015, http://www.abcam.com.

[38] Abnova, 2015, http://www.abnova.com.

[39] Novus Bio, 2015, http://www.novusbio.com.

[40] Ray Biotech, 2015, http://www.raybiotech.com.

[41] MyBioSource, 2015, http://www.mybiosource.com/product.php?name=elisa_kit.